Conductance scaling in Kondo-correlated quantum dots: Role of level asymmetry and charging energy

L. Merker,[1] S. Kirchner,[2,3] E. Muñoz,[4] and T. A. Costi[1]

[1]*Peter Grünberg Institut and Institute for Advanced Simulation, Research Centre Jülich, 52425 Jülich, Germany*

[2]*Max Planck Institute for the Physics of Complex Systems, 01187 Dresden, Germany*

[3]*Max Planck Institute for Chemical Physics of Solids, 01187 Dresden, Germany*

[4]*Facultad de Física, Pontificia Universidad Católica de Chile, Casilla 306, Santiago 22, Chile*

(Received 8 March 2013; published 24 April 2013)

The low-temperature electrical conductance through correlated quantum dots provides a sensitive probe of the physics (e.g., of Fermi-liquid versus non-Fermi-liquid behavior) of such systems. Here, we investigate the role of level asymmetry (gate voltage) and local Coulomb repulsion (charging energy) on the low-temperature and low-field scaling properties of the linear conductance of a quantum dot described by the single-level Anderson impurity model. We use the numerical renormalization group to quantify the regime of gate voltages and charging energies where universal Kondo scaling may be observed and also quantify the deviations from this universal behavior with increasing gate voltage away from the Kondo regime and with decreasing charging energy. We also compare our results with those from a recently developed method for linear and nonlinear transport, which is based on renormalized perturbation theory using dual fermions, finding excellent agreement at particle-hole symmetry and for all charging energies and reasonable agreement at small finite level asymmetry. Our results could be a useful guide for detailed experiments on conductance scaling in semiconductor and molecular quantum dots exhibiting the Kondo effect.

DOI: 10.1103/PhysRevB.87.165132 PACS number(s): 75.20.Hr, 71.27.+a, 72.15.Qm, 73.63.Kv

I. INTRODUCTION

Artificial nanostructures, such as semiconductor quantum dots,[1–4] magnetic atoms adsorbed on surfaces,[5–7] and molecules attached to leads,[8–12] provide new realizations of the Kondo effect of a local spin interacting antiferromagnetically with conduction electrons. In contrast to their bulk counterparts,[13] these systems are also highly tunable, for example, via application of gate voltages to modify the energy levels of the quantum dot or molecule, or to tune the tunnel couplings between the leads and the dot. In addition, application of a finite transport voltage allows an experimental investigation of the effects of strong correlations on nonequilibrium transport through these model nanosystems, thereby motivating also the development of new theoretical approaches for nonequilibrium.[14–26]

Motivated by recent experiments on conductance scaling in correlated quantum dots exhibiting the Kondo effect,[4,12,27] we present in this paper a detailed study of the low-temperature and low-field scaling properties of the linear conductance of a quantum dot described by the single-level Anderson impurity model. Scaling in physical properties is a hallmark of the Kondo effect.[13] Thus, a Kondo model description of a quantum dot implies that the conductance $G(T,B)$ is a universal function of T/T_0 and $g\mu_B B/k_B T_0$ over all temperatures T and magnetic fields B, with microscopic parameters (such as the Kondo exchange J) only entering through the dynamically generated low-energy scale T_0 (to be defined explicitly in Sec. III), with g, μ_B, k_B denoting the g factor, Bohr magneton, and Boltzmann's constant, respectively. In particular, for $T \ll T_0$ or $g\mu_B B \ll k_B T_0$, the functions $G(T,B=0) = G(0,0)[1 - c_T(T/T_0)^2]$ and $G(T = 0,B) = G(0,0)[1 - c_B(g\mu_B B/k_B T_0)^2]$ exhibit Fermi-liquid corrections about the unitary conductance $G(0,0)$ with deviations which are universal in the sense that the coefficients $c_T = \pi^4/16$ and $c_B = \pi^2/16$ are independent of microscopic details. Actual quantum dot devices, however, have a finite charging energy, and they are more realistically described by an Anderson model. The finite charging energy, and the ability to change the level energy of the quantum dot with a gate voltage, allow for charge fluctuations (even in the "Kondo regime" of the quantum dot) and can give rise to deviations from the expected Kondo scaling. It is therefore of some interest to quantify the effect of increasing charge fluctuations on the values of c_T and c_B. Recently, this issue has also been addressed in Ref. 25 by using a renormalized perturbation theory on the Keldysh contour[16,28] formulated using dual fermions.[29–31] This approach, denoted henceforth as superperturbation theory (SPT), yields both the linear and nonlinear conductance. In this paper, we shall compare the predictions of this theory for the linear conductance with results obtained within the numerical renormalization group (NRG) approach.[32–34]

The outline of the paper is as follows. Section II describes the quantum dot model. Section III gives a brief description of the calculation of the finite-temperature linear conductance $G(T,B)$ of the Anderson model within the NRG following the procedure in Ref. 35. In Sec. IV, some Fermi-liquid results for c_T and c_B are given, and in Sec. V we outline the SPT calculations of c_T and c_B, with which we shall compare. In Sec. VI, we present results for the dependence of the coefficients c_T and c_B on charging energy and gate voltage (local level energy). The latter are compared with the corresponding results from SPT. We conclude in Sec. VII with a discussion of the relevance of our results for experiments on quantum dots. In Appendix A, we give an alternative derivation of the discretization scheme of Campo *et al.* in Ref. 36, which we have used in the NRG calculations reported in this

paper. This derivation is carried out for an energy-dependent hybridization function following the procedure in Refs. 34 and 37. In Appendix B, we provide details of the SPT calculation of c_B in terms of renormalized parameters. The relation between bare and renormalized parameters, required for comparing SPT results for c_B and c_T with the NRG results, is also described in Appendix B.

II. MODEL

We consider the simplest model of a correlated quantum dot, the single-level Anderson model given by the Hamiltonian

$$H = \sum_{\sigma} \varepsilon_{d\sigma} n_{d\sigma} - g\mu_B B\, s_z^d + U n_{d\uparrow} n_{d\downarrow} + \sum_{k\alpha\sigma} \epsilon_{k\alpha} c^{\dagger}_{k\alpha\sigma} c_{k\alpha\sigma} + \sum_{k\alpha\sigma} (t_{\alpha} c^{\dagger}_{k\alpha\sigma} d_{\sigma} + \text{H.c.}). \quad (1)$$

Here, ε_d is the level energy, related to the gate voltage V_g in quantum dot via $\varepsilon_d \sim eV_g$ (see Fig. 1), B is a local magnetic field acting on the quantum dot with $s_z^d = \frac{1}{2}(n_{d\uparrow} - n_{d\downarrow})$, $U > 0$ is the Coulomb charging energy, σ labels the spin, and $\alpha = L, R$ labels left and right electron lead states with kinetic energies $\epsilon_{k\alpha}$. The couplings of the dot to the leads are denoted by $\Delta_{\alpha}(\omega) = \pi \rho_{\alpha}(\omega) |t_{\alpha}|^2$, where $\rho_{\alpha}(\omega) = \sum_k \delta(\omega - \epsilon_{k\alpha})$ is the density of states of lead α. For simplicity, we assume a constant density of states $\rho_{\alpha} = N_F = 1/2D$ with half-bandwidth $D = 1$ so that $\Delta_{\alpha} = \pi N_F t_{\alpha}^2$. By using even- and odd-parity combinations of left and right lead states, model (1) is reduced to a single-channel Anderson model with a resonant level half-width at half-maximum given by $\Delta = \Delta_L + \Delta_R$. The spectral function of the latter model is required in the calculation of the linear conductance, which we describe next.

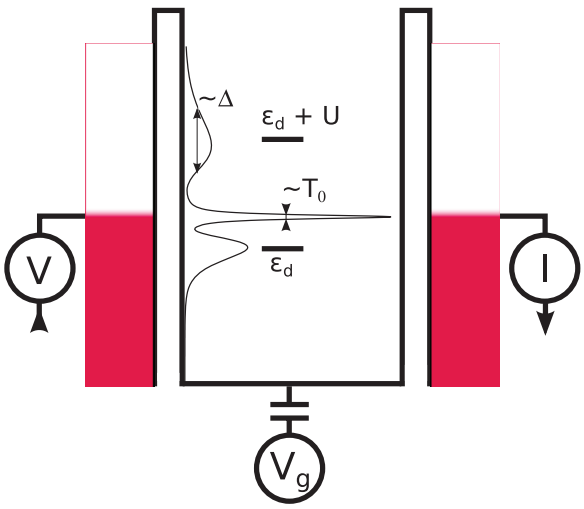

FIG. 1. (Color online) A strongly correlated quantum dot with charging energy $U \gg \Delta$ and level energy ε_d connected to leads via tunnel barriers. The gate voltage $V_g \sim \varepsilon_d$ allows changing occupation of the dot n_d from $n_d = 1$ for $\varepsilon_d = -U/2$ to $n_d = 0$ through a mixed valence regime with $n_d \approx 0.5$ for $\varepsilon_d \approx 0$. In the singly occupied configuration, shown here for $\varepsilon_d \approx -U/2$, the dot has a well-defined spin $\frac{1}{2}$ and the Coulomb blockade excitations at ε_d and $\varepsilon_d + U$ correspond to removing or adding an electron. The coupling of the spin $\frac{1}{2}$ to the leads results in the Kondo effect, which is manifested by the appearance of an additional many-body Kondo resonance at the Fermi level $\epsilon_F = 0$ at low temperatures $T \leqslant T_0$. This resonance is also reflected as a zero-bias anomaly in the nonlinear conductance dI/dV in experiments (Ref. 38).

III. NRG CALCULATION OF CONDUCTANCE

The linear response electrical conductance $G(T,B)$ of (1) is given by[39,40]

$$G(T,B) = \frac{e^2}{h} \int d\omega \left(-\frac{\partial f}{\partial \omega}\right) \sum_{\sigma} \mathcal{T}_{\sigma}(\omega,T,B), \quad (2)$$

where

$$\mathcal{T}_{\sigma}(\omega,T,B) = 4\pi \frac{\Delta_L \Delta_R}{\Delta_L + \Delta_R} A_{\sigma}(\omega,T,B) \quad (3)$$

is the transmission function for spin-σ electrons. It can be calculated from the single-particle spectral function of the dot $A_{\sigma}(\omega,T,B) = -\text{Im}[G_{d\sigma}(\omega + i\delta)]/\pi$, where $G_{d\sigma}(\omega + i\delta) = \langle\langle d_{\sigma}; d_{\sigma}^{\dagger} \rangle\rangle$ is the Fourier transform of the retarded single-particle Green's function of (1). In Eq. (2), e and h are the electronic charge and Planck's constant, respectively, and $f(\omega) = [1 + \exp(\beta\omega)]^{-1}$ is the Fermi function.

We use the NRG to evaluate the spectral function $A_{\sigma}(\omega,T,B)$ via the Lehmann representation

$$A_{\sigma}(\omega,T,B) = \frac{1}{Z} \sum_{m,n} |M_{mn}^{\sigma}|^2 (e^{-\beta E_m} + e^{-\beta E_n}) \times \delta[\omega - (E_m - E_n)], \quad (4)$$

where M_{mn}^{σ} are the matrix elements of the spin-σ local d-electron operator between eigenstates $|m\rangle$ and $|n\rangle$ with energies E_m and E_n and $Z = \sum_m \exp(-\beta E_m)$ is the partition function (see Ref. 34 for details). The usual approach is to broaden the discrete spectral function in Eq. (4) with Gaussians or logarithmic Gaussians in order to obtain a smooth function,[34,41,42] which is then substituted into Eq. (2), thereby yielding $G(T,B)$ after a numerical integration. A more accurate procedure, introduced in Ref. 35, is to substitute the discrete representation in Eq. (4) directly into Eq. (2), resulting in the expression

$$G(T,B) = \frac{\gamma\beta}{Z} \sum_{\sigma} \sum_{m,n} |M_{mn}^{\sigma}|^2 \frac{1}{e^{\beta E_m} + e^{\beta E_n}}, \quad (5)$$

where $\gamma = 4\pi \frac{e^2}{h} \frac{\Delta_L \Delta_R}{\Delta_L + \Delta_R}$. This avoids errors from numerical integrations and from an artificial broadening of the spectral function and has been shown to give accurate results for the conductance.[35] A similar procedure has been used in Ref. 43 to extract c_T for the symmetric Anderson model to within 5% accuracy. This uses a full density matrix evaluation of the spectral function[43,44] within the complete basis set[45] and is computationally more intensive than the approach which we use here, whose computational complexity is comparable to that of evaluating a local static correlation function.

For the remainder of this paper, we shall set the g factor g, Bohr magneton μ_B, Planck's constant h, electric charge e, and Boltzmanns constant k_B to unity, and also assume symmetric coupling to the leads ($\Delta_L = \Delta_R = \Delta/2$, $\gamma = \pi\Delta$). A finite asymmetry $\Delta_L \neq \Delta_R$ only influences the value of $G(0,0)$, but not our results for c_B and c_T. Note that in experiments on

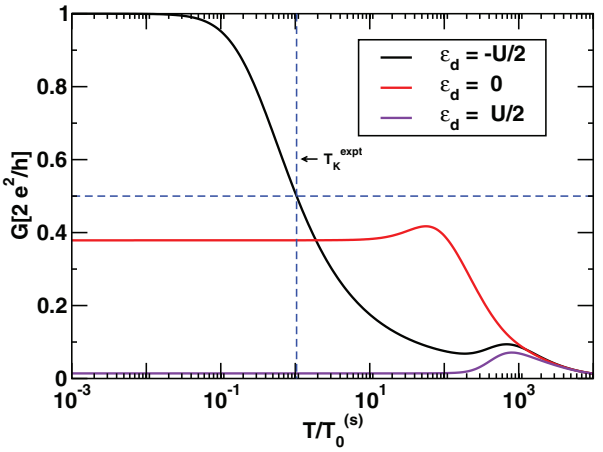

FIG. 2. (Color online) Linear conductance $G(T)$ versus T/T_0^s for $U/\Delta = 16$ and several values of $\varepsilon_d = -U/2,\ 0,\ +U/2$ using the approach of Ref. 35, with T_0^s defined by Eqs. (6) and (7). We also indicate with horizontal and vertical dashed lines the extraction of the experimental Kondo scale $T_K^{\rm expt}$ from the mid-valley Kondo conductance (i.e., that for $\varepsilon_d = -U/2$) via $G(T = T_K^{\rm expt}) = G(0)/2$. NRG parameters were for $\Lambda = 4$, with an energy cutoff $e_c(\Lambda = 4) = 30$ and $n_z = 2$.

quantum dots,[1,4] the extracted full width at half maximum of the Coulomb blockade peaks is given by $\Gamma = 2\Delta$.

In evaluating Eq. (5), we used z averaging[46] within the band discretization scheme of Ref. 36 (see Appendix A). A discretization parameter of $\Lambda = 4$ with $n_z = 2$ values for the z averaging was used and the cutoff for the rescaled energies at each NRG iteration was set to $e_c(\Lambda = 4) = 30$. Figure 2 shows typical examples for $G(T)$ versus T/T_0 at $B = 0$ for a strongly correlated quantum dot ($U/\Delta = 16 \gg 1$) in the Kondo ($\varepsilon_d = -U/2$), mixed valence ($\varepsilon_d = 0$), and empty orbital ($\varepsilon_d = U \gg \Delta$) regimes. The scale T_0 is defined from the $T = 0$ susceptibility of the Anderson model (1)

$$\chi(0) = 1/4T_0 \tag{6}$$

for all U and ε_d. For the case of particle-hole symmetry ($\varepsilon_d = -U/2$) and strong correlations $U \gg \pi\Delta$, one also has from the Bethe ansatz solution for $\chi(0)$ an analytic expression for T_0,

$$T_0(\varepsilon_d = -U/2) \equiv T_0^{(s)} \approx \sqrt{U\Delta/2}e^{-\pi U/8\Delta + \pi\Delta/2U}, \tag{7}$$

within corrections which are exponentially small in $U/\pi\Delta$ (see Ref. 13).

The Kondo scale T_0 is useful in analytic calculations of c_T and c_B about the Fermi-liquid fixed point at $T = 0$, such as those in Sec. IV. With this definition, the meaning of the coefficients c_T and c_B is fixed by

$$\frac{G(T, B = 0)}{G(0,0)} = 1 - c_T\left(\frac{T}{T_0}\right)^2 \quad (T \ll T_0), \tag{8}$$

$$\frac{G(T = 0, B)}{G(0,0)} = 1 - c_B\left(\frac{B}{T_0}\right)^2 \quad (B \ll T_0). \tag{9}$$

In extracting c_B, we do not use Eq. (9), but instead use the Fermi-liquid result in Eq. (17) of Sec. IV. This allows c_B to be obtained directly from the $T = 0$ occupancy of the d level, a quantity that can be calculated to high accuracy within the NRG. The coefficient c_T is extracted numerically by fitting $G(T,0)$ in the range $10^{-5}T_0 \leqslant T \leqslant 2 \times 10^{-2}T_0$ to the Fermi-liquid form in Eq. (8) with T_0 as defined in Eq. (6). The range $T \leqslant 0.02T_0$ was found optimal for this purpose, as we now describe.[47] Specifically, we fit the NRG results for $G(T,0)$ in the above range to $f(x) = a(1 - c_T x^2)$ where $x = T/T_0$. We find that $a = 2 \pm 10^{-5}$ at the particle-hole-symmetric point, with $a = 2$ (in units of e^2/h) being the exact result from the Friedel sum rule. The effect of the fitting range on the accuracy of the extracted c_T and the degree of confidence in the Fermi-liquid form $f(x) = a(1 - c_T x^2)$ may be ascertained quantitatively by calculating the R-squared coefficient R^2 (also called the coefficient of determination and defined in Table I). Table I lists R^2 together with the extracted c_T and the % error in c_T for different fitting ranges. We see that the range $10^{-5}T_0 \leqslant T \leqslant 0.02T_0$ is close to maximizing both R^2 and the accuracy of c_T [as compared to the exact result in Eq. (15) of Sec. IV]. We therefore used this range throughout, also for the asymmetric cases. Care is needed in the choice of the cutoff $e_c(\Lambda)$ in order to obtain correct results for $G(T)$ in the low-temperature limit when using Eq. (5). If $e_c(\Lambda)$ is chosen to be too small, the correct saturation behavior of $G(T,0)$ in the low-temperature limit (i.e., the "leveling off" of the conductance) is not obtained. In this case, a fit of $G(T,0)$ to $f(T/T_0)$ shows a drop in R^2 to small values, indicating a problem. This is remedied by increasing $e_c(\Lambda)$ [the used value $e_c(\Lambda = 4) = 30$ was sufficient, whereas $e_c(\Lambda = 4) = 12$, for example, is not]. Thus, the R^2 criterion can be a useful check on appropriate choices of cutoff when evaluating the conductance via Eq. (5).

TABLE I. Optimal temperature range for fitting the conductance $G(T,0)$ to the Fermi-liquid form $f(T/T_0) = a[1 - c_T(T/T_0)^2]$ for $U/\Delta = 12$ and $\varepsilon_d = -U/2$ using a goodness of fit based on the value of R^2. The latter is defined by $R^2 = 1 - \frac{\sum_{i=1}^n [y_i - f(x_i)]^2}{\sum_{i=1}^n (y_i - \langle y\rangle)^2}$, where $x_i = T_i/T_0$, $y_i = G(T_i,0)$, $\langle y\rangle = \frac{1}{n}\sum_{i=1}^n y_i$ and the number of data points in the fitting ranges was $n \approx 200$. The value $R^2 = 1$ would correspond to a perfect fit to the Fermi-liquid form. The % error in c_T in the last column is defined by % error $= 100 \cdot |\frac{c_T - c_{T,\rm exact}}{c_{T,\rm exact}}|$ where $c_{T,\rm exact}$ is the exact value at particle-hole symmetry given by Eq. (15). From this table, we see that the optimal range which maximizes R^2 and the accuracy of c_T is close to $T \leqslant 0.02T_0$. The NRG calculations used $\Lambda = 4$, $n_z = 2$, and an energy cutoff $e_c(\Lambda) = 30$.

Fitting range	R^2	c_T	% error
$10^{-5}T_0 \leqslant T \leqslant T_0$	0.818	0.7447	87
$10^{-5}T_0 \leqslant T \leqslant 0.1T_0$	0.9969	5.1277	16
$10^{-5}T_0 \leqslant T \leqslant 0.05T_0$	0.99965	5.8002	4.7
$10^{-5}T_0 \leqslant T \leqslant 0.02T_0$	0.999980	6.0820	0.086
$10^{-5}T_0 \leqslant T \leqslant 0.01T_0$	0.9999894	6.1459	0.96
$10^{-5}T_0 \leqslant T \leqslant 0.005T_0$	0.99985	6.1468	0.98
$10^{-5}T_0 \leqslant T \leqslant 0.001T_0$	0.9381	6.2034	1.91

In experiments on Kondo-correlated quantum dots, T_0 is not measurable, and instead one extracts a Kondo scale $T_K^{\rm expt}$ from the temperature dependence of the $B = 0$ conductance via

$$G\left(T = T_K^{\rm expt}\right) = G(0)/2. \tag{10}$$

In principle, this $T_{\mathrm{K}}^{\mathrm{expt}}$ can be extracted for each gate voltage (i.e., for each ε_d), but in practice, it is usually extracted only at mid-valley ($\varepsilon_d = -U/2$) where one is sure to be in the Kondo regime for large U/Δ. This is illustrated in Fig. 2 by the dashed lines.

With this definition of $T_{\mathrm{K}}^{\mathrm{expt}}$, one extracts the experimentally measured coefficients c_T^{expt} and c_B^{expt} via

$$\frac{G(T,B=0)}{G(0,0)} = 1 - c_T^{\mathrm{expt}} \left(\frac{T}{T_{\mathrm{K}}^{\mathrm{expt}}}\right)^2 \quad \left(T \ll T_{\mathrm{K}}^{\mathrm{exp}}\right), \tag{11}$$

$$\frac{G(T=0,B)}{G(0,0)} = 1 - c_B^{\mathrm{expt}} \left(\frac{B}{T_{\mathrm{K}}^{\mathrm{expt}}}\right)^2 \quad \left(B \ll T_{\mathrm{K}}^{\mathrm{exp}}\right). \tag{12}$$

For the particle-hole-symmetric Anderson model, the coefficients c_T^{expt} and c_B^{expt} are related to c_T and c_B via

$$c_T^{\mathrm{expt}} = c_T \left(\frac{T_{\mathrm{K}}^{\mathrm{expt}}}{T_0^{(s)}}\right)^2, \tag{13}$$

$$c_B^{\mathrm{expt}} = c_B \left(\frac{T_{\mathrm{K}}^{\mathrm{expt}}}{T_0^{(s)}}\right)^2. \tag{14}$$

For a precise translation of theoretical calculations of c_B and c_T in terms of T_0, into experimentally measured ones in terms of $T_{\mathrm{K}}^{\mathrm{expt}}$, one therefore requires the ratio $T_{\mathrm{K}}^{\mathrm{expt}}/T_0^s$ at mid-valley for all charging energies (U/Δ), which we supply in Sec. VI.

IV. FERMI-LIQUID RESULTS FOR $G(T,B)$

For the case of particle-hole symmetry, the coefficient c_T is known for arbitrary U/Δ within renormalized perturbation theory about the Fermi-liquid fixed point.[48] The expression is given by

$$c_T = \frac{\pi^4}{12}\frac{1+2(R-1)^2}{R^2}, \tag{15}$$

where R is the Wilson ratio [defined in Eq. (B24)]. In the limit of strong correlations $U/\Delta \gg 1$, the Wilson ratio approaches 2 and c_T takes the well-known universal Kondo value $c_T = \pi^4/16$ (see Refs. 49 and 50). In the opposite limit $U/\Delta \to 0$, the Wilson ratio tends to 1 and c_T acquires the value $\pi^4/12$. Evaluation of Eq. (15) for general U/Δ requires knowledge of R, either from Bethe ansatz or from NRG.

Fermi-liquid theory allows an exact analytic expression for c_B to be obtained for all U and ε_d. For this purpose, we use the Friedel sum rule $A_\sigma(0,B) = \sin^2[\pi n_{d\sigma}(B)]/\pi\Delta$, where $n_{d\sigma}(B)$ is the spin-σ local level occupancy in a small finite magnetic field $B \ll T_0$ at $T=0$. Using $n_{d\sigma}(B) = n_d/2 + \sigma\alpha B$, where n_d is the total occupancy at $B=0$, and the fact that $\alpha = \frac{1}{2}\frac{n_{d\uparrow}(B)-n_{d\downarrow}(B)}{B} = \chi(0)$ we easily find the exact result (correct to order B^2)

$$\frac{G(0,B)}{G(0,0)} = 1 - \pi^2\chi^2(0)B^2\left[1 - \cot^2\left(\frac{\pi n_d}{2}\right)\right]$$

$$= 1 - c_B\left(\frac{B}{T_0}\right)^2, \tag{16}$$

$$c_B = \frac{\pi^2}{16}\left[1 - \cot^2\left(\frac{\pi n_d}{2}\right)\right], \tag{17}$$

where $\chi(0) = 1/4T_0$ has been used. Note that at the particle-hole-symmetric point ($\varepsilon_d = -U/2$), where $n_d = 1$, c_B takes the universal Kondo value $\pi^2/16$ for all U.[51] This universal result [obtained also within SPT, see Eq. (19)] could be tested in semiconductor quantum dots that can be tuned through complete valleys. It would then acquire the value $\pi^2/16$ at mid-valley for any valley. The expression in Eq. (17) also shows that c_B decreases monotonically with increasing gate voltage away from mid-valley, with c_B becoming negative on entering the mixed valence regime (which we define by the average occupation being $n_d = 0.5$).

V. SPT CALCULATION

The SPT approach[25] is based on a renormalized perturbation theory on the Keldysh contour[16,28] using dual fermions.[29–31] This approach can be shown to be current conserving by construction[25] even in the nonlinear response regime, as opposed to finite-order perturbation theory in the bare parameters.[52] We compare the results of this theory for the linear conductance with NRG calculations. The reference system is the interacting particle-hole-symmetric Anderson model characterized by the renormalized Coulomb interaction $\tilde{u} = z\Gamma_0/\pi\Delta$, where z is the wave-function renormalization constant, and $\Gamma_0(U) \equiv \Gamma_{\uparrow,\downarrow;\downarrow,\uparrow}(0,0;0,0)$ the four-point vertex. In order to obtain results for the asymmetric model, an expansion in $\tilde{\varepsilon}_d \equiv z(\varepsilon_d + U/2)/z\Delta = (\varepsilon_d + U/2)/\Delta$ is carried out for the local level Green's function up to a given order in $\tilde{\varepsilon}_d$ and $\tilde{u}$, currently up to order $\tilde{u}^2\tilde{\varepsilon}_d^2$. As $z \to 0$ with increasing U/Δ such that in the symmetric case $\tilde{u} \to 1$, it follows that $\tilde{u}^2\tilde{\epsilon}_d^2$ increases with growing U/Δ at fixed ϵ_d/Δ. An outline of the method is presented in Appendix B, with full details available in the Supplemental Material of Ref. 25. The expression for c_T, given in Ref. 25, and that for c_B, derived in Appendix B, are given by

$$c_T' = \frac{\pi^4}{12}\frac{1+2\tilde{u}^2+(1-\tilde{u})(5\tilde{u}-3)\tilde{\varepsilon}_d^2}{(1+\tilde{u})^2\left[1+(1-\tilde{u})^2\tilde{\varepsilon}_d^2\right]^2}, \tag{18}$$

$$c_B' = \frac{\pi^2}{16}\frac{1-3(1-\tilde{u})^2\tilde{\varepsilon}_d^2}{\left[1+(1-\tilde{u})^2\tilde{\varepsilon}_d^2\right]^2}, \tag{19}$$

where the apostrophe on these indicates that they are evaluated by using the susceptibility Kondo scale of the reference system (symmetric Anderson model), i.e., c_T', c_B' are defined via

$$\frac{G(T,B=0)}{G(0,0)} = 1 - c_T'\left(\frac{T}{T_0^{(s)}}\right)^2 \quad \left(T \ll T_0^s\right), \tag{20}$$

$$\frac{G(T=0,B)}{G(0,0)} = 1 - c_B'\left(\frac{B}{T_0^{(s)}}\right)^2 \quad \left(B \ll T_0^s\right), \tag{21}$$

where $T_0^{(s)} = 1/4\chi(0)$ is the susceptibility Kondo scale for the symmetric model and is given explicitly within SPT by Eq. (B18). In order to compare the above results with those from NRG, we need to relate the renormalized Coulomb interaction $\tilde{u}$, appearing in the former, to the bare Coulomb interaction U, appearing in the latter. As outlined in Appendix B, from Eq. (B25) this relation is given by $\tilde{u} = R - 1$ for the symmetric Anderson model, where the Wilson ratio R is calculated for given U/Δ from the exact Bethe

ansatz expressions for the susceptibility and specific heat[53] of the fully interacting symmetric Anderson model.[54] Notice that upon substituting $\tilde{u} = R - 1$ into the SPT expression (18), for the particle-hole symmetric limit $\tilde{\varepsilon}_d = 0$, it reduces to the exact Fermi-liquid result (15).

VI. RESULTS

A. Symmetric case ($\varepsilon_d = -U/2$)

Figure 3 shows c_T versus U for the symmetric model, both in terms of the scale $T_0(\varepsilon_d = -U/2) \equiv T_0^{(s)}$ and in terms of the Kondo scale from the conductance $T_K^{\rm expt}$ (i.e., $c_T^{\rm expt}$, discussed below). The former is compared with the corresponding SPT prediction in Eq. (18) and we see very good agreement between this and the NRG calculations for all U/Δ. For $U/\Delta \gtrsim 6$, the value of c_T remains within 2% of the the universal Kondo value $c_T = \pi^4/16 = 6.088$. The value $U/\Delta = \pi \approx 3$ separates the weakly correlated ($U/\pi\Delta < 1$) from the strongly correlated regime ($U/\pi\Delta > 1$).[13] We see that in the moderately correlated regime $6 \gtrsim U/\Delta \gtrsim 1$, the deviation c_T from the Kondo value increases, eventually reaching 7% at $U/\Delta \approx 3$. For weakly correlated (non-Kondo) quantum dots with $U/\pi\Delta \lesssim 1$, c_T first decreases with decreasing U, reaches a minimum at $U/\Delta \approx 1.7$, and then increases to its noninteracting value of $\pi^4/12 \approx 8.117$ at $U = 0$. Note that this latter value differs by more than 30% from the Kondo value at $U \gg \Delta$.

In Fig. 3(a), we show the ratio $T_K^{\rm expt}/T_0^{(s)}$ versus U. This ratio allows obtaining $c_T^{\rm expt}$ from Eq. (13), the coefficient measured in experiments, and which we show in Fig. 3. Note the very different behavior between $c_T^{\rm expt}$ and c_T for charging energies $U/\Delta \lesssim 5$. This is due to the strong dependence of $T_K^{\rm expt}/T_0^{(s)}$ on U/Δ in this range of charging energies. In particlular, $c_T^{\rm expt}$ acquires a maximum value of ≈ 8.75 at $U/\Delta \approx 3.5$. Since $T_K^{\rm expt}/T_0^{(s)} \approx 1.041$ for $U/\Delta \gtrsim 10$ [Fig. 3(a)], $c_T^{\rm expt} \approx 6.58$ for strongly correlated quantum dots in the Kondo regime.[55] In contrast, for $U/\Delta \lesssim 10$, the scale $T_K^{\rm expt}$ differs appreciably from $T_0^{(s)}$. Thus, even for nominally Kondo-correlated quantum dots with $U/\Delta \approx 4.5$, such as those in Ref. 4, one finds from Fig. 3(a) that $T_K^{\rm expt}/T_0^{(s)} \approx 1.18$, so one should expect $c_T^{\rm expt} \approx 7.5$, which is somewhat larger than the extracted value $c_T^{\rm expt} \approx 5.6 \pm 1.2$.[4]

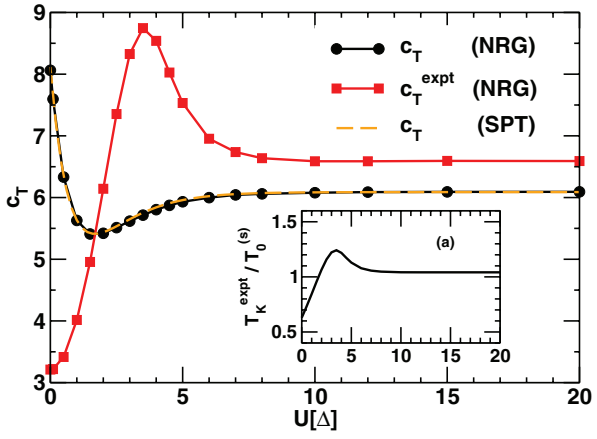

FIG. 3. (Color online) c_T vs U/Δ for the symmetric Anderson model calculated within NRG (solid lines with symbols) and SPT (dashed line). Filled circles show c_T using the susceptibility scale $T_0^{(s)}$, while filled squares show c_T upon using the scale from the conductance $T_K^{\rm expt}$. By comparing the value of c_T at $U/\Delta \gg 1$ with the exact one $c_T = \pi^4/16 \approx 6.088$, we estimate the relative error in the NRG calculation of c_T to lie below 0.2%, considerably more accurate than previous estimates (Refs. 43 and 50). Inset (a): ratio $T_K^{\rm expt}/T_0^{(s)}$ vs U/Δ. For $U/\Delta \gg 1$, the ratio $T_K^{\rm expt}/T_0^{(s)}$ approaches 1.04. NRG parameters were for $\Lambda = 4$ with an energy cutoff $e_c(\Lambda = 4) = 30$ and $n_z = 2$.

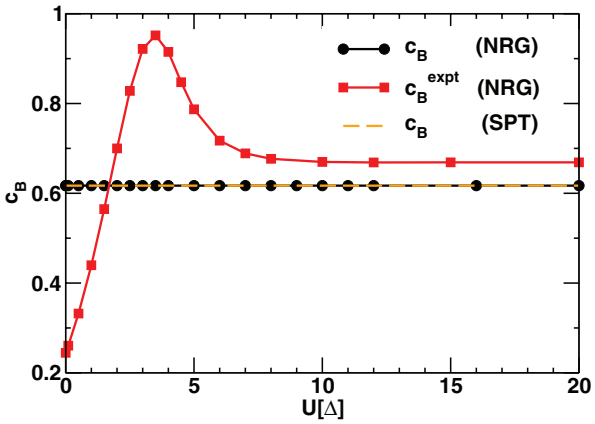

FIG. 4. (Color online) c_B (filled circles) and $c_B^{\rm expt}$ (filled squares) vs U/Δ for the symmetric Anderson model calculated within NRG parameters were for $\Lambda = 4$ with an energy cutoff $e_c(\Lambda = 4) = 30$ and $n_z = 2$. SPT (dashed curve) also recovers the value $c_B = \pi^2/16$ for particle-hole symmetry.

As discussed in Sec. IV, c_B is independent of the charging energy U for the particle-hole-symmetric case, where it takes the value $\pi^2/16 \approx 0.617$, which is also recovered exactly within SPT [see Eq. (19)]. However, experiments use the scale $T_K^{\rm expt}$ and measure $c_B^{\rm expt}$ as given by Eq. (14). This depends on U through the ratio of Kondo scales $T_K^{\rm expt}/T_0^{(s)}$. For completeness, we therefore show the U dependence of $c_B^{\rm expt}$ in Fig. 4. For $U/\Delta \approx 4.5$, relevant for the experiments in Ref. 4, we find $c_B^{\rm expt} \approx 0.89$ significantly smaller than the value $c_B^{\rm expt} \approx 5.1$ extracted from the measurements. As discussed in that paper, the large discrepancy between the measured and predicted values of $c_B^{\rm expt}$ could indicate the importance of the large spin-orbit interaction present in the InAs quantum dots investigated in Ref. 4.

B. Asymmetric case ($\varepsilon_d > -U/2$)

1. NRG results

For completeness, we show the dependence of c_T on ε_d for $\varepsilon_d \geqslant -U/2$ for U ranging from weakly ($U/\Delta \ll 1$) to strongly ($U/\Delta \gg 1$) correlated quantum dots in Fig. 5. For strong correlations $U/\Delta \gg 1$, c_T decreases monotonically with increasing deviations from the Kondo regime, eventually becoming negative after the mixed valence regime is reached. A similar behavior is seen in the local level dependence of c_B, shown in Fig. 6. In Fig. 6(a), we show the ratio c_T/c_B versus ε_d/Δ for selected U/Δ which approaches the value

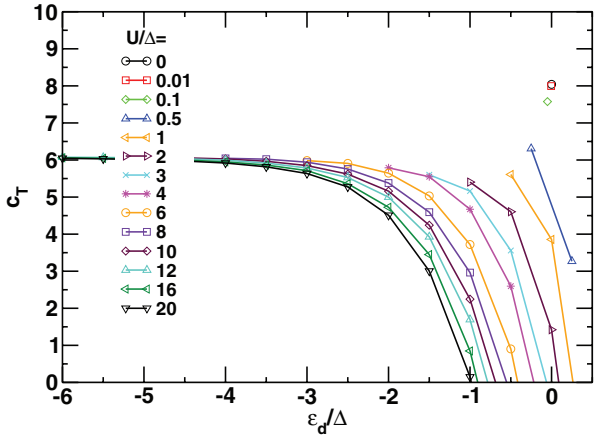

FIG. 5. (Color online) c_T vs ε_d (in intervals of 0.5Δ) with $\varepsilon_d \geqslant -U/2$ for several U/Δ, ranging from strong $U \gg \Delta$ to weak $U \ll \Delta$ correlations, and using the scale T_0. NRG parameters were for $\Lambda = 4$ with an energy cutoff $e_c(\Lambda = 4) = 30$ and $n_z = 2$.

π^2 at particle-hole symmetry and $U/\Delta \gg 1$. Notice that for correlated quantum dots in the Kondo regime, c_T/c_B decreases monotonically with increasing deviation from particle-hole symmetry. Since c_T/c_B is independent of the definition of Kondo scale used, it could be a useful quantity to quantify the degree of correlations in a quantum dot (U/Δ) and the degree of departure from particle-hole symmetry for specific gate voltages.

2. *Comparison with SPT*

Figure 7 compares SPT results for the local level dependence of c'_T, as defined in Eqs. (18) and (20), with correspondingly defined quantities in NRG. Figure 8 shows a similar comparison for the quantity c'_B defined in Eqs. (19) and (21). We see in both cases that agreement between NRG and SPT holds for $\tilde{\varepsilon}_d \equiv (\varepsilon_d + U/2)/\Delta \lesssim 0.25$, which is consistent with the SPT calculations carried out to order $\tilde{u}^2\tilde{\varepsilon}_d^2$. For larger

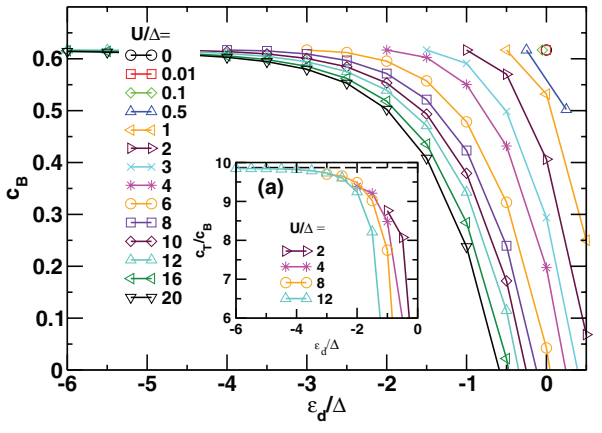

FIG. 6. (Color online) c_B vs ε_d (in intervals of 0.5Δ) with $\varepsilon_d \geqslant -U/2$ for several U/Δ, ranging from strong $U \gg \Delta$ to weak $U \ll \Delta$ correlations, and using the scale T_0. NRG parameters were for $\Lambda = 4$ with an energy cutoff $e_c(\Lambda = 4) = 30$ and $n_z = 2$. Inset (a) shows c_T/c_B vs ε_d/Δ for selected U/Δ. The dashed line is a guide to the eye and represents the universal Kondo value $c_T/c_B = \pi^2$ reached in the limit $U/\Delta \to \infty$ and particle-hole symmetry.

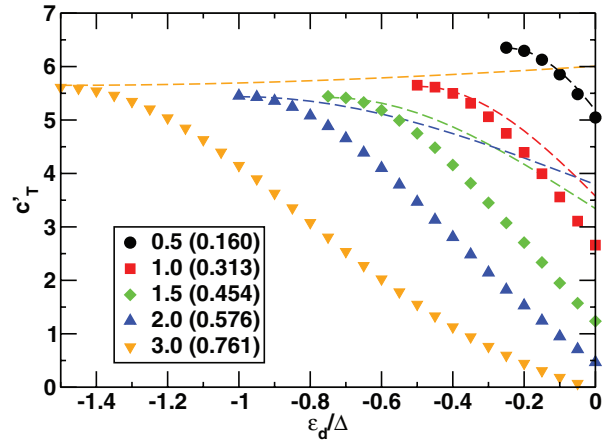

FIG. 7. (Color online) c'_T vs ε_d/Δ for several U/Δ calculated within NRG (symbols) and SPT (lines). Legend: column one U/Δ, column two $\tilde{u}$. c'_T is defined in Eq. (18) using the Kondo scale in Eq. (20), and the corresponding NRG result uses the same Kondo scale for the purposes of this comparison. NRG parameters were for $\Lambda = 4$ with an energy cutoff $e_c(\Lambda = 4) = 30$ and $n_z = 2$.

deviations from the symmetric point and with increasing Coulomb interactions, we see an increasing deviation of the SPT results from the NRG calculations. In contrast to the NRG calculation, we also see that the SPT result for c'_T ceases to decrease monotonically with $\tilde{\varepsilon}_d$ for $U/\Delta \gtrsim 3$ (corresponding to a renormalized Coulomb interaction $\tilde{u} \gtrsim 0.76$). On the other hand, the SPT result for c'_B decreases monotonically with increasing $\tilde{\varepsilon}_d$ as in the corresponding NRG result. Although we show comparisons also in the region $\tilde{\varepsilon}_d \gg 1$, by construction the SPT calculation is perturbative in $\tilde{\varepsilon}_d$ and agreement can only be expected in the limit $\tilde{\varepsilon}_d \ll 1$, which we find. We also expect that the range of agreement between NRG and SPT in both $\tilde{u}$ and $\tilde{\varepsilon}_d$ can be increased by going to higher order (see discussion at the end of Appendix B 4), however, this lies beyond the scope of this paper.

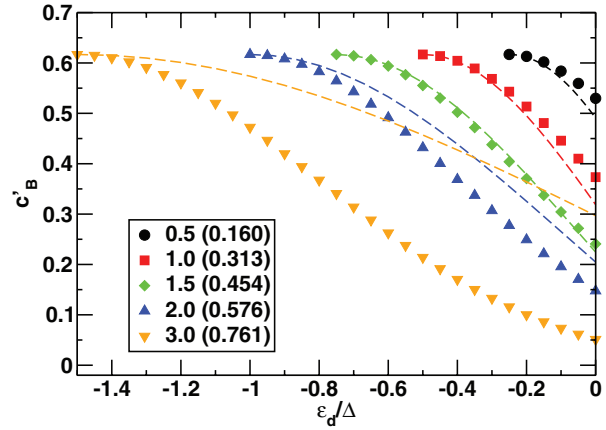

FIG. 8. (Color online) c_B vs ε_d/Δ for several U/Δ calculated within NRG (symbols) and SPT (lines). Legend: column one U/Δ, column two $\tilde{u}$. c'_B is defined in Eq. (19) using the Kondo scale in Eq. (21), and the corresponding NRG result uses the same Kondo scale for the purposes of this comparison. NRG parameters were for $\Lambda = 4$ with an energy cutoff $e_c(\Lambda = 4) = 30$ and $n_z = 2$.

VII. CONCLUSIONS

In this paper, we investigated deviations from the universal Kondo scaling in the linear conductance of a correlated quantum dot due to a finite level asymmetry (i.e., deviation of gate voltage from mid-valley) and a finite local Coulomb repulsion (i.e., finite charging energy). In particular, we determined the behavior of the coefficients c_T and c_B as a function of ε_d and U within NRG and compared these with results from SPT,[25] finding good agreement for all U at the symmetric point and reasonable agreement for $\tilde{\varepsilon}_d = (\varepsilon_d + U/2)/\Delta \lesssim 0.25$ away from the symmetric point. Both c_T and c_B are monotonically decreasing functions of the deviation $\tilde{\varepsilon}_d$ from the symmetric point $\tilde{\varepsilon}_d = 0$ for all U, and an exact Fermi-liquid expression for c_B has been given which is valid for any U and ε_d. In particular, the coefficients c_T and c_B become negative on entering the mixed valence regime, signaling the onset of thermally activated transport which becomes pronounced in the empty orbital limit $n_d \approx 0$.

For the mid-valley conductance, we also determined the ratio of the conductance to susceptibility Kondo scales $T_{\mathrm{K}}^{\mathrm{expt}}/T_0^{(s)}$, allowing us to relate our results for c_T and c_B in terms of $T_0^{(s)}$ to the measured coefficients c_T^{expt} and c_B^{expt} in terms of $T_{\mathrm{K}}^{\mathrm{expt}}$. While for quantum dots with $U/\Delta \gtrsim 6$, the difference between the two sets of coefficients is a constant factor of order unity [e.g., $c_{T,B}^{\mathrm{expt}}/c_{T,B} = (T_{\mathrm{K}}^{\mathrm{expt}}/T_0^{(s)})^2 \approx 1.08$ for $U/\Delta \gg 6$], for quantum dots with $U/\Delta \lesssim 6$ this difference becomes significant and should be carefully taken into account in detailed comparisons of theory with experiment. We expect this to be particularly important for semiconducting quantum dots since U/Δ is tunable to smaller values in these systems.

ACKNOWLEDGMENTS

T.A.C. and L.M. thank A. Weichselbaum for some useful comments on this work and acknowledge supercomputer support by the John von Neumann Institute for Computing (Jülich). E.M. and S.K. acknowledge support by the Comisión Nacional de Investigación Científica y Tecnológica (CONICYT), Grant No. 11100064 and the German Academic Exchange Service (DAAD) under Grant No. 52636698.

APPENDIX A: ALTERNATIVE DERIVATION OF THE CAMPO DISCRETIZATION

In this Appendix, we give a derivation of the discretization scheme of Ref. 36, following the procedure for general energy-dependent hybridization functions of Bulla *et al.* in Refs. 34 and 37, which has been used for the NRG calculations of the conductance in this paper.

We start with the single-channel Anderson impurity model, given by

$$H = H_{imp} + \sum_{k,\sigma} \epsilon_{k,\sigma} c_{k,\sigma}^\dagger c_{k,\sigma} + \sum_{k,\sigma} V_k (f_\sigma^\dagger c_{k,\sigma} + c_{k,\sigma}^\dagger f_\sigma),$$

which may be written in the energy representation as[37]

$$H = H_{imp} + \sum_\sigma \int_{-D_-}^{D_+} h(\epsilon)(f_\sigma^\dagger a_{\epsilon,\sigma} + a_{\epsilon,\sigma}^\dagger f_\sigma) d\epsilon + \sum_\sigma \int_{-D_-}^{D_+} g(\epsilon) a_{\epsilon,\sigma}^\dagger a_{\epsilon,\sigma} d\epsilon. \tag{A1}$$

Here, $a_{\epsilon,\sigma}$ and $a_{\epsilon',\sigma'}^\dagger$ obey the standard anticommutation relations $\{a_{\epsilon,\sigma}, a_{\epsilon',\sigma'}^\dagger\} = \delta_{\sigma,\sigma'}\delta(\epsilon - \epsilon')$, $g(\epsilon)$ is the dispersion, $h(\epsilon)$ is the hybridization amplitude, and $\pm D_\pm$ are the upper/lower conduction electron band edges. The model (A1) is characterized by the hybridization function $\Delta(\omega) = \sum_k |V_k|^2 \delta(\omega - \epsilon_k)$. As shown in Ref. 37, its energy dependence may be distributed arbitrarily over the functions $g(\epsilon)$ and $h(\epsilon)$, as long as the following condition is satisfied:

$$\Delta(\omega) = \pi \frac{d\epsilon(\omega)}{d\omega} h[\epsilon(\omega)]^2, \tag{A2}$$

where $\epsilon(\omega)$ is the inverse function of the dispersion $g(\epsilon)$, i.e.,

$$g[\epsilon(\omega)] = \omega.$$

Our starting point is the observation by Campo *et al.*[36] that a linear discretization of the conduction band with a Fourier basis in the discrete intervals leads to a correct estimate for $\Delta(\omega)$, whereas a Fourier decomposition on a logarithmic scale as suggested by Krishna-Murthy *et al.* in Ref. 33 systematically underestimates $\Delta(\omega)$ [or equivalently the conduction electron density of states $\rho(\omega)$ since $\Delta(\omega) = \pi\rho(\omega)V^2$ for a constant hybridization matrix element $V_k = V$]. This underestimation results in an effective hybridization function $\tilde{\Delta}(\omega) = \Delta(\omega)/A_\Lambda$ where the factor $A_\Lambda = \frac{\ln\Lambda}{2}\frac{1+\Lambda^{-1}}{1-\Lambda^{-1}} > 1$ is due the discretization and $\Lambda > 1$ is the band discretization parameter.[56] While this effect may be corrected "manually" for each Λ, it is clearly advantageous to have a built-in procedure within the NRG that does this automatically. Campo *et al.* accomplished this within a logarithmic discretization scheme by using a Fourier decomposition in terms of nonorthogonal basis functions. As in the case of the linear grid, this correctly estimated $\Delta(\omega)$. Motivated by this, we provide here an alternative derivation of this discretization scheme following the procedure of Bulla *et al.* in Refs. 34 and 37 for general $\Delta(\omega)$.

We consider the following set of orthonormal Fourier functions in each interval of a linear grid:

$$\psi_{n,p}(\eta) = \begin{cases} e^{-2\pi i p \eta}, & \text{if } \eta \in [n, n+1], \quad n = -1, 0, 1, \ldots \\ 0, & \text{otherwise.} \end{cases}$$

The inverse functions are given by $\Psi_{n,p}(\eta) = \psi_{n,p}^*(\eta)$ fulfilling the usual orthonormality condition

$$\int_{-\infty}^{\infty} \psi_{n,p}(\eta)\Psi_{n',p'}(\eta) d\eta = \delta_{n,n'}\delta_{p,p'}. \tag{A3}$$

We will transform this relation to a logarithmic grid such that $[n, n+1]$ will be transformed to $D_+[\Lambda^{-n-z-1}, \Lambda^{-n-z}]$ for $n = 0, 1, \ldots$. The first interval $[-1, 0]$ is special and transforms to the first logarithmic interval containing the band edge, i.e., to $D_+[\Lambda^{-z}, 1]$. One possible choice, the obvious one, is $\epsilon = D_+\Lambda^{-\eta-z} \leftrightarrow \eta(\epsilon) = -\ln|\epsilon/D_+|/\ln\Lambda - z, n = 0, 1, \ldots$ ($\epsilon = D_+\Lambda^{-z(\eta+1)}$, $n = -1$), but other choices are possible for defining the transformation between linear and logarithmic grids [and hence $\eta(\epsilon)$].[57] Thus, for $n = 0, 1, \ldots$, we have[58]

$$\int_0^\infty \underbrace{\frac{1}{|\epsilon|\ln\Lambda}\psi_{n,p}\left(-\frac{\ln\frac{|\epsilon|}{D_+}}{\ln\Lambda} - z\right)}_{=\phi_{n,p}^+(\epsilon)/c_n^+} \underbrace{\Psi_{n',p'}\left(-\frac{\ln\frac{|\epsilon|}{D_+}}{\ln\Lambda} - z\right)}_{=c_n^+\cdot\Phi_{n',p'}^+(\epsilon)} d\epsilon = \delta_{n,n'}\delta_{p,p'}. \tag{A4}$$

For the expansion of the negative part of the band, we use $\epsilon = -D_-\Lambda^{-\eta-z}$ and do not reverse the integration boundaries yielding the same function inside the integration

$$\int_{-\infty}^{0} \underbrace{\frac{1}{|\epsilon|\ln\Lambda}\psi_{n,p}\left(-\frac{\ln\frac{|\epsilon|}{D_-}}{\ln\Lambda}-z\right)}_{=\phi^-_{n,p}(\epsilon)/c^-_n} \underbrace{\Psi_{n',p'}\left(-\frac{\ln\frac{|\epsilon|}{D_-}}{\ln\Lambda}-z\right)}_{=c^-_n\cdot\Phi^-_{n',p'}(\epsilon)} d\epsilon = \delta_{n,n'}\delta_{p,p'}. \tag{A5}$$

The normalization factor $c^\pm_n$ can be distributed freely between the new basis $\phi^\pm_{n,p}$ and its inverse $\Phi^\pm_{n,p}$. $a_{\epsilon,\sigma}$ is expressed in terms of the new basis

$$a_{\epsilon,\sigma} = \sum_{n,p} a_{n,p,\sigma}\phi^+_{n,p}(\epsilon) + b_{n,p,\sigma}\phi^-_{n,p}(\epsilon),$$

where

$$a_{n,p,\sigma} = \int^{+n} a_{\epsilon,\sigma}\Phi^+_{n,p}(\epsilon)d\epsilon, \quad b_{n,p,\sigma} = \int^{-n} b_{\epsilon,\sigma}\Phi^-_{n,p}(\epsilon)d\epsilon,$$

where we defined

$$\int^{+n} = \int_{D_+\Lambda^{-n-z-1}}^{D_+\Lambda^{-n-z}}, \quad \int^{-n} = \int_{-D_-\Lambda^{-n-z}}^{-D_-\Lambda^{-n-z-1}}.$$

Evaluating the anticommutator $\{a_{n,p,\sigma}, a^\dagger_{n',p',\sigma'}\}$ we find

$$\begin{aligned}
&\{a_{n,p,\sigma}, a^\dagger_{n',p',\sigma'}\} \\
&= \int^{+n} a_{\epsilon,\sigma}\Phi^+_{n,p}(\epsilon)d\epsilon \int^{+n'} a^\dagger_{\epsilon',\sigma'}{\Phi^+_{n',p'}}^*(\epsilon')d\epsilon' \\
&\quad + \int^{+n'} a^\dagger_{\epsilon',\sigma'}{\Phi^+_{n',p'}}^*(\epsilon')d\epsilon \int^{+n} a_{\epsilon,\sigma}\Phi^+_{n,p}(\epsilon)d\epsilon \\
&= \delta_{n,n'}\int^{+n}\int^{+n}[a_{\epsilon,\sigma}, a^\dagger_{\epsilon',\sigma'}]\Phi^+_{n,p}(\epsilon){\Phi^+_{n,p'}}^*(\epsilon')d\epsilon\, d\epsilon' \\
&= \delta_{n,n'}\delta_{\sigma,\sigma'}\int^{+n}\Phi^+_{n,p}(\epsilon){\Phi^+_{n,p'}}^*(\epsilon)d\epsilon \\
&= \delta_{n,n'}\delta_{\sigma,\sigma'}\int^{+n}\frac{1}{|c^+_n|^2}e^{2\pi i(p-p')\left(\frac{\ln\frac{|\epsilon|}{D_\pm}}{\ln\Lambda}+z\right)}
\end{aligned}$$

with an analogous expression for $\{b_{n,p,\sigma}, b^\dagger_{n',p',\sigma'}\}$. Setting $\{a_{n,p,\sigma}, a^\dagger_{n,p,\sigma}\} = \{b_{n,p,\sigma}, b^\dagger_{n,p,\sigma}\} = 1$ fixes the constants $c^\pm_n$ in Eqs. (A4) and (A5), leading to

$$\begin{aligned}
|c^\pm_n|^2 &= D_\pm\Lambda^{-n-z}(1-\Lambda^{-1}) = d^\pm_n \\
&[= D_\pm(1-\Lambda^{-z}) \quad \text{for } n=-1]
\end{aligned}$$

and

$$\{a_{n,p,\sigma}, a^\dagger_{n',p',\sigma'}\} = \delta_{n,n'}\delta_{\sigma,\sigma'}\begin{cases}1, & \text{if } p=p'\\ \frac{\ln\Lambda}{2\pi i(p-p')+\ln\Lambda}, & \text{otherwise}\end{cases}$$

with an analogous expression for $\{b_{n,p,\sigma}, b^\dagger_{n',p',\sigma'}\}$. Thus, only for the continuum limit $\Lambda \to 1$ is the above an orthonormal basis for all p, p'.[36] However, as we show in the following, an approximate discretized Hamiltonian can be formulated in terms of the orthonormal subset of $p=0$ states only, within which the NRG calculation is carried out. We show that for general $\Delta(\omega)$, (i) only $p=0$ states couple to the impurity, and (ii) off-diagonal terms in p, p' can always be eliminated from the Hamiltonian by a suitable choice of the function $\eta(\epsilon)$ relating the linear to the logarithmic discretization $\epsilon = \pm D_\pm\Lambda^{-\eta(\epsilon)-z}$.

With the new basis functions, we follow the derivation of Bulla *et al.* in Ref. 34, reformulating first the hybridization part of Eq. (A1):

$$\begin{aligned}
\int_{-D_-}^{D_+} h(\epsilon)a_{\epsilon,\sigma}d\epsilon &= \sum_{n,p} a_{n,p,\sigma}\int^{+n} h(\epsilon)\phi^+_{n,p}(\epsilon)d\epsilon \\
&\quad + \sum_{n,p} b_{n,p,\sigma}\int^{-n} h(\epsilon)\phi^-_{n,p}(\epsilon)d\epsilon.
\end{aligned}$$

The requirement that the hybridization only couples to the $p=0$ terms can be satisfied by choosing $h(\epsilon) \propto \Phi^\pm_{n,0}(\epsilon) = \frac{1}{\sqrt{d^\pm_n}}$, which by Eqs. (A4) and (A5) implies that $p \neq 0$ do not hybridize. Therefore, we can choose the same $h(\epsilon)$ as in Ref. 34 (i.e., a step function in the discrete intervals):

$$h(\epsilon)^2 \equiv h^{\pm 2}_n = \frac{1}{d^\pm_n}\int^{\pm n}\frac{1}{\pi}\Delta(\omega)d\omega \tag{A6}$$

for $D_\pm\Lambda^{-n-z} < \pm\epsilon < D_\pm\Lambda^{-n-1-z}$. This choice guarantees that $\epsilon(\pm D_\pm\Lambda^{-n-z}) = \pm D_\pm\Lambda^{-n-z}$ [proved by using Eqs. (A2) and (A6)] and that the dispersion is linear at the grid points $g(\pm D_\pm\Lambda^{-n-z}) = \pm D_\pm\Lambda^{-n-z}$. The first part of the hybridization may be written as

$$\begin{aligned}
\sum_\sigma\int_{-D_-}^{+D_+} h(\epsilon)f^\dagger_\sigma a_{\epsilon,\sigma}d\epsilon &= \frac{1}{\sqrt{\pi}}\sum_n f^\dagger_\sigma(\gamma^+_n a_{n,0,\sigma} + \gamma^-_n b_{n,0,\sigma}) \\
&\equiv \sqrt{\frac{\xi_0}{\pi}}\sum_\sigma f^\dagger_\sigma f_{0\sigma},
\end{aligned}$$

where $\gamma^{\pm 2}_n = \int^{\pm n}\Delta(\omega)d\omega$, and the conduction electron Wannier orbital at the impurity site is defined as $f_{0\sigma} = \frac{1}{\sqrt{\xi_0}}\sum_n \gamma^+_n a_{n,0,\sigma} + \gamma^-_n b_{n,0,\sigma}$, with $\xi_0 = \sum_n(\gamma^+_n)^2 + (\gamma^-_n)^2$.

Next, we reformulate the conduction electron kinetic energy term

$$\begin{aligned}
&\int_{-D_-}^{D_+} g(\epsilon)a^\dagger_{\epsilon,\sigma}a_{\epsilon,\sigma}d\epsilon \\
&\quad = \sum_n\sum_{p,p'} a^\dagger_{n,p,\sigma}a_{n,p',\sigma}\int^{+n} g(\epsilon)\phi^+_{n,p}(\epsilon){\phi^+_{n,p'}}^*(\epsilon)d\epsilon \\
&\qquad + b^\dagger_{n,p,\sigma}b_{n,p',\sigma}\int^{-n} g(\epsilon)\phi^-_{n,p}(\epsilon){\phi^-_{n,p'}}^*(\epsilon)d\epsilon \\
&\quad = \sum_n\sum_{p,p'} a^\dagger_{n,p,\sigma}a_{n,p',\sigma}\xi^+_{n,p,p'} + b^\dagger_{n,p,\sigma}b_{n,p',\sigma}\xi^-_{n,p,p'}, \\
\xi^\pm_{n,p,p'} &= \int^{\pm n} g(\epsilon)\phi^\pm_{n,p}(\epsilon){\phi^\pm_{n,p'}}^*(\epsilon)d\epsilon \\
&= \int^{\pm n}\omega\Delta(\omega)\frac{1}{\pi h(\epsilon)^2}\phi^\pm_{n,p}(\epsilon){\phi^\pm_{n,p'}}^*(\epsilon)d\omega \\
&= \frac{\int^{\pm n}\omega\Delta(\omega)d^\pm_n\phi^\pm_{n,p}[\epsilon(\omega)]{\phi^\pm_{n,p'}}^*[\epsilon(\omega)]d\omega}{\int^{\pm n}\Delta(\omega)d\omega} \\
&= \frac{\int^{\pm n}\frac{\omega\Delta(\omega)d^{\pm 2}_n}{[|\epsilon(\omega)|\ln\Lambda]^2}e^{2\pi i(p-p')\left(\frac{\ln\frac{|\epsilon(\omega)|}{D_\pm}}{\ln\Lambda}+z\right)}d\omega}{\int^{\pm n}\Delta(\omega)d\omega}.
\end{aligned}$$

For $\Delta(\omega)=\Delta_0$, we obtain $\epsilon(\omega)=\omega$ and only $\xi^{\pm}_{n,p=p'}=\pm\frac{d^{\pm}_n}{\ln\Lambda}$ are unequal to zero and agree with the result of Campo and Oliveira. Thus, the impurity, which by construction couples only to the $p=0$ state via the hybridization term, is completely decoupled from the $p\neq 0$ states. We now show that the same can be achieved for a general $\Delta(\omega)$ by a suitable choice of $\eta(\epsilon)$.

Following the same derivation as above, but substituting

$$\eta(\epsilon)=\int_{k_n^{(2)}}^{\epsilon}\frac{k_n^{(1)}}{g(\epsilon')}d\epsilon' \tag{A7}$$

in Eq. (A3) leads to diagonal $\xi_{n,p,p'}$ for an arbitrary $\Delta(\omega)$. $k_n^{(1)}$ and $k_n^{(2)}$ are given by the boundary conditions $\int_{k_n^{(2)}}^{\pm D_\pm\Lambda^{-n-z}}\frac{k_n^{(1)}}{g(\epsilon')}d\epsilon=n$ and $\int_{k_n^{(2)}}^{\pm D_\pm\Lambda^{-n-z-1}}\frac{k_n^{(1)}}{g(\epsilon')}d\epsilon=n+1$. $c_n^{\pm}$ and $\gamma_n^{\pm}$ remain unchanged, but

$$\begin{aligned}\xi^{\pm}_{n,p,p'}&=\int^{\pm n}g(\epsilon)\phi^{\pm}_{n,p}(\epsilon)\phi^{\pm}_{n,p'}{}^{*}(\epsilon)d\epsilon\\&=\int^{\pm n}\frac{d_n^{\pm}k_n^{(1)2}}{g(\epsilon)}e^{2\pi i(p-p')\int_{k_n^{(2)}}^{\epsilon}\frac{k_n^{(1)}}{g(\epsilon')}d\epsilon'}d\epsilon\\&=\mp k_n^{(1)}d_n^{\pm}\delta_{p,p'}.\end{aligned}$$

$k_n^{(1)}$ can be obtained by taking the difference of the boundary conditions (as defined above), and using $\epsilon(\pm D_\pm\Lambda^{-n-z})=\pm D_\pm\Lambda^{-n-z}$ and Eq. (A2),

$$k_n^{(1)}=\frac{\int^{\pm n}\Delta(\omega)d\omega}{\mp d_n^{\pm}\int^{\pm n}\frac{\Delta(\omega)}{\omega}d\omega}.$$

As in Ref. 36, the resulting $\xi^{\pm}_{n,p=p'}\equiv\xi^{\pm}_{n,p=p'}(C)$ are given by[59]

$$\xi^{\pm}_{n,p=p'}(C)=\frac{\int^{\pm n}\Delta(\omega)d\omega}{\int^{\pm n}\frac{\Delta(\omega)}{\omega}d\omega}. \tag{A8}$$

The corresponding result, denoted by $\xi^{\pm}_{n,p=p'}=\xi^{\pm}_{n,p=p'}(B)$, in the usual logarithmic discretization scheme is given by[37,60]

$$\xi^{\pm}_{n,p=p'}(B)=\frac{\int^{\pm n}\omega\Delta(\omega)d\omega}{\int^{\pm n}\Delta(\omega)d\omega}. \tag{A9}$$

Evaluating (A8) and (A9) for a flat band with $D_+=D_-=1$ gives

$$\begin{aligned}&\xi^{\pm}_{n,p=p'}(C)=\pm\tfrac{1}{2}(1+\Lambda^{-1})\Lambda^{-n-z}/A_\Lambda,\quad n=0,1,\ldots\\&\xi^{\pm}_{n,p=p'}(C)=\pm\tfrac{1}{2}(1+(\Lambda^z)^{-1})/A_{\Lambda^z},\quad n=-1\\&\xi^{\pm}_{n,p=p'}(B)=\pm\tfrac{1}{2}(1+\Lambda^{-1})\Lambda^{-n-z},\quad n=0,1,\ldots\\&\xi^{\pm}_{n,p=p'}(B)=\pm\tfrac{1}{2}[1+(\Lambda^z)^{-1}],\quad n=-1.\end{aligned}$$

We see that $\xi^{\pm}_{n,p=p'}(B)/\xi^{\pm}_{n,p=p'}(C)$ is given by the factor A_Λ (A_{Λ^z} for $n=-1$), indicating that the Campo discretization achieves the correct estimate for $\Delta(\omega)$ via a reduction of the effective bandwidth of the discretized model. For energies close to the band edge, where the Campo discretization gives a different correction to the desired one (A_{Λ^z} instead of A_Λ), further corrections are needed.[61]

APPENDIX B: SPT CALCULATION OF c_B

We describe the system by the single-impurity Anderson Hamiltonian $\hat{H}=\hat{H}_c+\hat{H}_d+\hat{H}_{d-c}$, where we defined

$$\begin{aligned}\hat{H}_c&=\sum_{\lambda=L,R}\sum_{k,\sigma}\epsilon_{k\lambda}\hat{c}^{\dagger}_{k\lambda\sigma}\hat{c}_{k\lambda\sigma},\\\hat{H}_d&=\sum_{\sigma}E_{d,\sigma}\hat{d}^{\dagger}_{\sigma}\hat{d}_{\sigma}+U\left(\hat{d}^{\dagger}_{\uparrow}\hat{d}_{\uparrow}-\frac{1}{2}\right)\left(\hat{d}^{\dagger}_{\downarrow}\hat{d}_{\downarrow}-\frac{1}{2}\right)-\frac{U}{4},\\\hat{H}_{d-c}&=\sum_{\lambda=L,R}\sum_{k,\sigma}(V_{k\lambda}\hat{d}^{\dagger}_{\sigma}\hat{c}_{k\lambda\sigma}+V^{*}_{k\lambda}\hat{c}^{\dagger}_{k\lambda\sigma}\hat{d}_{\sigma}).\end{aligned} \tag{B1}$$

Here, $\hat{H}_c$ is the single-band Hamiltonian for conduction electrons at the metallic leads. H_d is the Hamiltonian for localized quasiparticle states at the dot, which includes Coulomb interaction. $\hat{H}_{d-c}$ represents the coupling between the dot and the leads. We have defined the spin-dependent local energy level $E_{d\sigma}=E_d-\sigma b$, with $E_d=\epsilon_d+U/2$ a small parameter to capture deviations from the particle-hole symmetric condition $\epsilon_d=-U/2$, and $b=g\mu_B B/2$. We build up an SPT calculation starting from a reference system which is interacting ($U\neq 0$), particle-hole symmetric ($E_d=\epsilon_d+U/2=0$), and in the absence of an external magnetic field ($B=0$).

1. Reference system

The reference system ($E_d=0$, $B=0$) self-energy was derived in detail in Ref. 25, and is given by the matrix form

$$\Sigma_{\sigma,\omega}=\begin{bmatrix}\Sigma^{--}_{\sigma,\omega}&-\Sigma^{-+}_{\sigma,\omega}\\-\Sigma^{+-}_{\sigma,\omega}&\Sigma^{++}_{\sigma,\omega}\end{bmatrix}.$$

The local Green's function for the reference system is given by the matrix

$$\mathbf{g}_{\sigma,\omega}=\begin{bmatrix}g^{--}_{\sigma,\omega}&g^{-+}_{\sigma,\omega}\\g^{+-}_{\sigma,\omega}&g^{++}_{\sigma,\omega}\end{bmatrix},$$

with components satisfying[25]

$$\begin{aligned}g^{--}_{\sigma,\omega}&=[1-F(\omega,T,V)]g^{r}_{\sigma,\omega}+F(\omega,T,V)g^{a}_{\sigma,\omega},\\g^{-+}_{\sigma,\omega}&=-F(\omega,T,V)\left[g^{r}_{\sigma,\omega}-g^{a}_{\sigma,\omega}\right],\\g^{+-}_{\sigma,\omega}&=[1-F(\omega,T,V)]\left[g^{r}_{\sigma,\omega}-g^{a}_{\sigma,\omega}\right],\\g^{++}_{\sigma,\omega}&=-[1-F(\omega,T,V)]g^{a}_{\sigma,\omega}-F(\omega,T,V)g^{r}_{\sigma,\omega}.\end{aligned} \tag{B2}$$

Here, the effective local nonequilibrium distribution function is shown[25] to be

$$F(\omega,T,V)=\frac{\Delta_L f_L+\Delta_R f_R-(i/2)\Sigma^{-+}_{\omega}}{\Delta_L+\Delta_R-\mathrm{Im}\Sigma^{r}_{\omega}}.$$

The retarded component of the Green's function is given by

$$g^{r}_{\sigma\omega}=\left(\omega+i\Delta-\Sigma^{r}_{\omega}\right)^{-1},$$

with $g^{a}_{\sigma\omega}=[g^{r}_{\sigma\omega}]^{*}$, and $\Delta=\Delta_L+\Delta_R$. It is shown in Ref. 25 that the self-energy components for the reference system satisfy a similar set of relations as Eq. (B2), in particular with

$$\begin{aligned}\Sigma^{-+}_{\omega}&=-2i\,\mathrm{Im}\Sigma^{r}_{\omega}F(\omega,T,V),\\\Sigma^{+-}_{\omega}&=2i\,\mathrm{Im}\Sigma^{r}_{\omega}[1-F(\omega,T,V)].\end{aligned}$$

The (spin-independent) retarded self-energy of the reference system was calculated in detail in Ref. 25, and is given by

$$\Sigma^r_\omega = (1-\tilde{\chi}_{++})\omega - i\Delta\frac{\tilde{\chi}^2_{+-}}{2}\left[\left(\frac{\omega}{\Delta}\right)^2+\left(\frac{\pi T}{\Delta}\right)^2 + \zeta\left(\frac{eV}{\Delta}\right)^2 - \tilde{\chi}^2_{++}\frac{\zeta}{3}\left(\frac{\pi T eV}{\Delta^2}\right)^2\right] \quad \text{(B3)}$$

with $\Sigma^a_\omega = (\Sigma^r_\omega)^*$. In Eq. (B3), the "odd" component of the spin susceptibility is directly related to the four-point vertex $\Gamma_0(U)$ defined in Eq. (B12) by the relation $\tilde{\chi}_{+-}(U) = \Gamma_0/(\pi\Delta)$.

2. SPT formulation

A coherent-states path-integral representation of the model of Eq. (B1) in terms of Grassmann fields can be obtained following the standard construction. On the Keldysh contour, we introduce $\hat{\psi}_{k\lambda\sigma}(t)^\dagger = [c^-_{k\lambda\sigma}(t), c^+_{k\lambda\sigma}(t)]^\dagger$ and $\hat{\Phi}(t)^\dagger = [d^-_\sigma(t), d^+_\sigma(t)]^\dagger$, where the indexes $\pm$ refer to the time-ordered $(-)$ and anti-time-ordered $(+)$ paths, while $\lambda = \{L,R\}$ labels the two different leads.

The resulting nonequilibrium generating functional for the model of Eq. (B1) is[25,62]

$$Z = \int \mathcal{D}[\hat{\psi}^\dagger,\hat{\psi}]\mathcal{D}[\hat{\Phi}^\dagger,\hat{\Phi}]e^{iS[\hat{\psi}^\dagger,\hat{\psi},\hat{\Phi}^\dagger,\hat{\Phi}]}. \quad \text{(B4)}$$

Since the action in Eq. (B4) is Gaussian in the $\hat{\psi}^\dagger_{k\lambda\sigma}(t)$, $\hat{\psi}_{k\lambda\sigma}(t)$ Grassmann fields, we integrate those in the partition function (B4) to obtain, in the frequency-space representation,

$$Z = \int \mathcal{D}[\hat{\Phi}^\dagger_{\sigma\omega},\hat{\Phi}_{\sigma\omega}]e^{iS[\hat{\Phi}^\dagger_{\sigma\omega},\hat{\Phi}_{\sigma\omega}]}. \quad \text{(B5)}$$

In Eq. (B5), we have defined the effective action as

$$iS[\hat{\Phi}^\dagger_{\sigma\omega},\hat{\Phi}_{\sigma\omega}] = iS_U[\hat{\Phi}^\dagger_{\sigma\omega},\hat{\Phi}_{\sigma\omega}] - i\int_{-\infty}^{+\infty}\frac{d\omega}{2\pi}\sum_\sigma \hat{\Phi}^\dagger_{\sigma\omega}E_{d\sigma}\hat{\sigma}_3\hat{\Phi}_{\sigma\omega},$$

where

$$iS_U[\hat{\Phi}^\dagger_{\sigma\omega},\hat{\Phi}_{\sigma\omega}] = iS^{int}_U[\hat{\Phi}^\dagger_{\sigma\omega},\hat{\Phi}_{\sigma\omega}] + i\int_{-\infty}^{+\infty}\frac{d\omega}{2\pi}\sum_\sigma \hat{\Phi}^\dagger_{\sigma\omega}[\omega + i(\Delta_L+\Delta_R)]\hat{\sigma}_3\hat{\Phi}_{\sigma\omega} \quad \text{(B6)}$$

is the effective action for a particle-hole-symmetric ($E_d = 0$) and interacting ($U \neq 0$) system in the absence of an external magnetic field ($B = 0$), and

$$i\Delta_\lambda = -\sum_{k,\sigma}\frac{|V_{k\lambda}|^2}{\omega - \epsilon_{k\lambda} + i\eta^+} \quad \text{for } \lambda = L,R$$

is the coupling with the metallic leads, which in the limit of a flat band [$\rho^\lambda(\omega) = \rho^\lambda_0$, $V_{k\lambda} = V_\lambda$] of infinite bandwidth, tends to $i\Gamma_\lambda \to i\pi\rho^\lambda_0|V_\lambda|^2$. In order to construct a perturbation theory in the small parameters E_d, B, with respect to the reference system defined by the action (B6), let us introduce the dual fermion (Grassmann) fields $\hat{\phi}^\dagger_{\sigma\omega} = (f^-_{\sigma\omega}, f^+_{\sigma\omega})^\dagger$ where, as before, the index $\mp$ refers to the time-ordered (anti-time-ordered) path along the Keldysh contour. We insert the fermionic Hubbard-Stratonovich transformation[29,30]

$$\int \mathcal{D}[\hat{\phi}^\dagger_{\sigma\omega},\hat{\phi}_{\sigma\omega}]\exp\left\{i\sum_\sigma\int_{-\infty}^{+\infty}\frac{d\omega}{2\pi}[\hat{\phi}^\dagger_{\sigma\omega}(\mathbf{g}_{\sigma\omega}E_{d\sigma}\hat{\sigma}_3\mathbf{g}_{\sigma\omega})^{-1} \times \hat{\phi}_{\sigma\omega} - \hat{\phi}^\dagger_{\sigma\omega}\mathbf{g}^{-1}_{\sigma\omega}\hat{\Phi}_{\sigma\omega} - \hat{\Phi}^\dagger_{\sigma\omega}\mathbf{g}^{-1}_{\sigma\omega}\hat{\phi}_{\sigma\omega}]\right\}$$
$$= \mathrm{Det}[(\mathbf{g}_{\sigma\omega}E_{d\sigma}\hat{\sigma}_3\mathbf{g}_{\sigma\omega})^{-1}]e^{-i\sum_\sigma\int_{-\infty}^{+\infty}\frac{d\omega}{2\pi}\hat{\Phi}^\dagger_{\sigma\omega}E_{d\sigma}\hat{\sigma}_3\hat{\Phi}_{\sigma,\omega}}$$

into the partition function (B5). Integrating out the local fermion field $\hat{\Phi}_{\sigma\omega}$, one finds that the dual fermion bare Green's function is given by[25]

$$\mathbf{G}^{f(0)}_{\sigma\omega} = -\mathbf{g}_{\sigma\omega}\left(\mathbf{g}_{\sigma\omega} - E^{-1}_{d\sigma}\hat{\sigma}_3\right)^{-1}\mathbf{g}_{\sigma\omega}. \quad \text{(B7)}$$

On the other hand, by functional differentiation of the partition function, an exact nonperturbative relation between the dual fermion dressed Green's function $G^{f,ij}_{\sigma\omega} = -i\langle\hat{\phi}^{i\dagger}_{\sigma\omega}\hat{\phi}^j_{\sigma\omega}\rangle$ and the local Green's function $G^{ij}_{\sigma\omega} = -i\langle\hat{\Phi}^{i\dagger}_{\sigma\omega}\hat{\Phi}^j_{\sigma\omega}\rangle$ is obtained[25]:

$$\mathbf{G}_{\sigma,\omega} = -E^{-1}_{d\sigma}\hat{\sigma}_3 + (\mathbf{g}_{\sigma,\omega}E_{d\sigma}\hat{\sigma}_3)^{-1}\mathbf{G}^f_{\sigma,\omega}(E_{d\sigma}\hat{\sigma}_3\mathbf{g}_{\sigma,\omega})^{-1}. \quad \text{(B8)}$$

The dual fermion Green's function satisfies the matrix Dyson equation[25]

$$\mathbf{G}^f_{\sigma,\omega} = \mathbf{G}^{f(0)}_{\sigma,\omega} + \mathbf{G}^{f(0)}_{\sigma,\omega}\Sigma^f_{\sigma\omega}\mathbf{G}^f_{\sigma,\omega}. \quad \text{(B9)}$$

Notice that the zeroth-order solution of Eqs. (B9) and (B8) is

$$\mathbf{G}^{(0)}_{\sigma\omega} = -E_{d\sigma}\hat{\sigma}_3 + (\mathbf{g}_{\sigma\omega}E_{d\sigma}\hat{\sigma}_3)^{-1}\mathbf{G}^{f(0)}_{\sigma\omega}(E_{d\sigma}\hat{\sigma}_3\mathbf{g}_{\sigma\omega})^{-1} = \left(\mathbf{g}^{-1}_{\sigma\omega} - E_{d\sigma}\hat{\sigma}_3\right)^{-1}.$$

The first-order solution for the Dyson equation (B9) is

$$\mathbf{G}^{f(1)}_{\sigma,\omega} = \mathbf{G}^{f(0)}_{\sigma,\omega} + \mathbf{G}^{f(0)}_{\sigma,\omega}\Sigma^f_{\sigma,\omega}\mathbf{G}^{f(0)}_{\sigma,\omega},$$

which upon substitution into Eq. (B8) yields

$$\mathbf{G}^{(1)}_{\sigma,\omega} = \mathbf{G}^{(0)}_{\sigma,\omega} + \mathbf{G}^{(0)}_{\sigma,\omega}\Sigma^f_{\sigma,\omega}\mathbf{G}^{(0)}_{\sigma,\omega} = \left[\mathbf{G}^{(0)\,-1}_{\sigma,\omega} - \Sigma^f_{\sigma,\omega}\right]^{-1} + O([\Sigma^f]^2) = \left[\mathbf{g}^{(0)\,-1}_{\sigma,\omega} - \Sigma_{\sigma,\omega} - E_{d\sigma}\hat{\sigma}_3 - \Sigma^f_{\sigma,\omega}\right]^{-1}.$$

It is clear then that, within this first-order solution of the Dyson equation, the perturbed matrix self-energy is given by

$$\Sigma_{\sigma,E_d}(\omega,B) = (E_d + \sigma b)\hat{\sigma}_3 + \Sigma_{\sigma,\omega} + \Sigma^f_{\sigma,\omega}. \quad \text{(B10)}$$

3. Dual fermion self-energy

In order to simplify the notation, let us use the multi-indexed labels $1 \equiv (\omega_1,\sigma_1,i_1)$ for frequency, spin, and Keldysh contour $i_1 = \mp$ indices. Let us define

$$D_{12} \equiv (2\pi)\delta_{\omega_1-\omega_2}\delta_{\sigma_1,\sigma_2}E_{d\sigma_1}[\hat{\sigma}_3]_{i_1,i_2},$$
$$g_{12} \equiv (2\pi)\delta_{\omega_1-\omega_2}\delta_{\sigma_1,\sigma_2}g^{i_1,i_2}_{\sigma_1\omega_1},$$
$$\Gamma_{1234} \equiv (2\pi)\delta_{\omega_1+\omega_3-\omega_2-\omega_4}[\Gamma_{\sigma_1\sigma_2;\sigma_3\sigma_4}(\omega_1,\omega_2;\omega_3,\omega_4)]^{i_1,i_2;i_3,i_4}.$$

Here, $\Gamma_{\sigma_1\sigma_2;\sigma_3\sigma_4}(\omega_1,\omega_2;\omega_3,\omega_4)$ is the four-point vertex of the reference system. The dual fermion self-energy is given by the expression

$$\Sigma^f_{12} \equiv (2\pi)\delta_{\omega_1-\omega_2}\delta_{\sigma_1,\sigma_2}\left[\Sigma^f_{\sigma_1,\omega_1}\right]_{i_1,i_2} = i\Gamma_{1234}g_{44'}[g - D^{-1}]^{-1}_{4'3'}g_{3'3},$$

where in this context repeated indices stand for a generalized convolution in frequency, spin, and Keldysh-contour indices.

A series expansion of the dual fermion self-energy matrix follows from $[g - D^{-1}]^{-1} = -D[I - gD]^{-1} = -D - DgD - DgDgD + \ldots$:

$$\Sigma^f_{12} = -i\Gamma_{1234}\,[gDg]_{43} - i\Gamma_{1234}\,[gDgDg]_{43} + O(D^3). \tag{B11}$$

The four-point vertex is given by

$$\Gamma^{(0)----}_{\sigma\sigma';\sigma'\sigma} = \Gamma_0(1-\delta_{\sigma,\sigma'}), \quad \Gamma^{(0)++++}_{\sigma\sigma';\sigma'\sigma} = -\Gamma_0(1-\delta_{\sigma,\sigma'}),$$

where

$$\Gamma_0(U) = U + \pi\Delta(15 - 3\pi^2/2)(U/\pi\Delta)^3 + O(U^5). \tag{B12}$$

The first term on the right-hand side of Eq. (B11) possesses only two nonvanishing diagonal matrix elements,

$$\begin{aligned} &-i\sum_{\sigma',j=\pm}\int\frac{d\omega'}{2\pi}\Gamma^{(0)-----}_{\sigma\sigma';\sigma'\sigma}\,g^{-j}_{\sigma'\omega'}E_{d\sigma'}[\hat{\sigma}_3]_{jj}\,g^{j-}_{\sigma'\omega'} \\ &\quad = -i\Gamma_0 E_{d,-\sigma}Z^{--}_{-\sigma}, \end{aligned}$$

and $+i\Gamma_0 E_{d,-\sigma}Z^{++}_{-\sigma}$, where we have defined

$$Z^{--}_\sigma = \int_{-\infty}^{+\infty}\frac{d\omega'}{2\pi}([g^{--}_{-\sigma\omega'}]^2 - g^{-+}_{-\sigma\omega'}g^{+-}_{-\sigma\omega'})$$

and $Z^{++}_\sigma = (Z^{--}_\sigma)^*$. Direct calculation of the integral, and consistently with the approximation for the reference system keeping terms up to $O(\Gamma_0^2)$ only, we obtain

$$\begin{aligned} \Sigma^{f,--}_\sigma(\omega,B) &= -i\Gamma_0 E_{d,-\sigma}Z^{--}_{-\sigma} \\ &= -(E_d+\sigma b)\tilde{u}\left\{1 - \frac{1}{3}\left[\left(\frac{\pi T}{\tilde{\Delta}}\right)^2 + \left(\frac{eV}{\tilde{\Delta}}\right)^2\right]\right. \\ &\quad \left. + \frac{7}{9}\zeta\left(\frac{\pi T eV}{\tilde{\Delta}^2}\right)^2\right\}, \end{aligned} \tag{B13}$$

with the other components given by $\Sigma^{f,++}_\sigma(\omega,B) = -\Sigma^{f,--}_\sigma(\omega,B)$, $\Sigma^{f,+-}_\sigma(\omega,B) = \Sigma^{f,-+}_\sigma(\omega,B) = 0$.

4. Retarded self-energy

At the order of approximation of Eqs. (B10) and (B13),[25] the self-energy components at the local site are

$$\begin{aligned} \Sigma^{++}_{\sigma,E_d}(\omega,B) &= \Sigma^{++}_{\sigma\omega} - E_{d\sigma} + \Sigma^{f,++}_\sigma(\omega,B), \\ \Sigma^{--}_{\sigma,E_d}(\omega,B) &= \Sigma^{--}_\sigma(\omega,B) + E_{d\sigma} + \Sigma^{f,--}_\sigma(\omega,B), \\ \Sigma^{+-}_{\sigma,E_d}(\omega,B) &= \Sigma^{+-}_\sigma(\omega,B), \\ \Sigma^{-+}_{\sigma,E_d}(\omega,B) &= \Sigma^{-+}_\sigma(\omega,B). \end{aligned} \tag{B14}$$

We thus obtain the retarded self-energy from the relation $\Sigma^r_{\sigma,E_d}(\omega,B) = \Sigma^{+-}_{\sigma,E_d}(\omega,B) - \Sigma^{++}_{\sigma,E_d}(\omega,B)$ as follows:

$$\begin{aligned} &\Sigma^r_{\sigma,E_d}(\omega,B) \\ &\quad = (1-\tilde{\chi}_{++})\omega + E_d - \sigma b - (E_d+\sigma h)\tilde{u} \\ &\quad\times\left\{1 - \frac{1}{3}\left[\left(\frac{\pi T}{\tilde{\Delta}}\right)^2 + \left(\frac{eV}{\tilde{\Delta}}\right)^2\right] + \frac{7}{9}\zeta\left(\frac{\pi T eV}{\tilde{\Delta}^2}\right)^2\right\} \\ &\quad + i\Delta\tilde{u}^2\left[\left(\frac{\omega}{\tilde{\Delta}}\right)^2 + \left(\frac{\pi T}{\tilde{\Delta}}\right)^2 + \zeta\left(\frac{eV}{\tilde{\Delta}}\right)^2 - \frac{\zeta}{3}\left(\frac{\pi T eV}{\tilde{\Delta}^2}\right)^2\right]. \end{aligned} \tag{B15}$$

Here, $\tilde{u} = z\Gamma_0/(\pi\Delta)$ is the renormalized interaction, for $z = \tilde{\chi}^{-1}_{++}$ the wave-function renormalization factor for the particle-hole-symmetric reference system at zero magnetic field. The renormalized quasiparticle spectral broadening is $\tilde{\Delta} = z\Delta$. The retarded Green's function corresponding to this self-energy is

$$\begin{aligned} G^r_{\sigma,E_d}(\omega,B) &= [\omega + i\Delta - \Sigma^r_{\sigma,E_d}(\omega,B)]^{-1} \\ &= \tilde{\chi}^{-1}_{++}(\omega - \tilde{E}_d + \sigma\tilde{b} + i\tilde{\Delta} - \tilde{\Sigma}^r_{\sigma\omega}(B))^{-1}. \end{aligned}$$

Here, we have defined the renormalized self-energy

$$\begin{aligned} \tilde{\Sigma}^r_{\sigma\omega}(B) &= -(\tilde{E}_d + \sigma\tilde{b})\tilde{u}\left\{1 - \frac{1}{3}\left[\left(\frac{\pi T}{\tilde{\Delta}}\right)^2 + \left(\frac{eV}{\tilde{\Delta}}\right)^2\right]\right. \\ &\quad \left. + \frac{7}{9}\zeta\left(\frac{\pi T eV}{\tilde{\Delta}^2}\right)^2\right\} + i\tilde{\Delta}\tilde{u}^2\left[\left(\frac{\omega}{\tilde{\Delta}}\right)^2 + \left(\frac{\pi T}{\tilde{\Delta}}\right)^2\right. \\ &\quad \left. + \zeta\left(\frac{eV}{\tilde{\Delta}}\right)^2 - \frac{\zeta}{3}\left(\frac{\pi T eV}{\tilde{\Delta}^2}\right)^2\right]. \end{aligned}$$

In the above, we have systematically included all contributions up to second order in the renormalized Coulomb interaction $\tilde{u}$ and particle-hole asymmetry $\tilde{\varepsilon}_d = \tilde{E}_d/\tilde{\Delta} = E_d/\Delta$. This corresponds to approximating the dual fermion Green's function by

$$\mathbf{G}^f = \mathbf{G}^f_0 + \mathbf{G}^f_0\,\Sigma^f\,\mathbf{G}^f_0 \tag{B16}$$

instead of a self-consistent solution of the Dyson equation $\mathbf{G}^f = \mathbf{G}^f_0 + \mathbf{G}^f_0\,\Sigma^f\,\mathbf{G}^f$. The self-energy in this equation involves a single renormalized four-point vertex, as stated by Eq. (B11). Additional contributions to the self-energy are generated by including reducible contributions to the four-point vertex. This involves the entire family of "parquet" diagrams. Explicit calculations of these higher-order contributions are currently under development, but go beyond the scope of this paper.

5. Differential conductance $G(T,B)$

The differential conductance $G(T,B) \equiv dI/dV$ is expressed by the formula

$$G(T,B) = \frac{e^2}{h}\int_{-\infty}^{+\infty}d\omega\left(-\frac{\partial f}{\partial\omega}\right)\sum_\sigma \mathcal{T}_\sigma(\omega,T,B).$$

Here, the transmission is

$$\mathcal{T}_\sigma(\omega,T,B) = 4\pi\frac{\Delta_L\Delta_R}{\Delta_L+\Delta_R}A_\sigma(\omega,T,B),$$

where the spectral function is defined as

$$A_\sigma(\omega,T,B) = -\frac{1}{\pi}\mathrm{Im}G^r_{\sigma,E_d}(\omega,B).$$

The differential conductance at zero bias, and up to second order in temperature and magnetic field, can be cast into the form

$$\frac{G(T,B)}{G_0} = 1 - c'_T\left(\frac{T}{T_0^{(s)}}\right)^2 - c'_B\left(\frac{g\mu_B B/2}{k_B T_0^{(s)}}\right)^2. \tag{B17}$$

Here, the Kondo scale is based on the spin susceptibility of the particle-hole-symmetric system $\chi^s(0) = (g\mu_B)^2/4T_0^{(s)}$, with

$$\chi^s(0) = \frac{(g\mu_B)^2}{2}\tilde{A}_d(0)(1+\tilde{U}\tilde{A}_d(0)) = \frac{(g\mu_B)^2}{2}\frac{1}{\pi\tilde{\Delta}}\left(1+\frac{\tilde{U}}{\pi\tilde{\Delta}}\right) = \frac{(g\mu_B)^2}{2}\frac{1}{\pi\tilde{\Delta}}(1+\tilde{u}),$$

and we have used $\tilde{A}_d(0) = 1/(\pi\tilde{\Delta})$. Thus,

$$T_0^{(s)} = \frac{\pi\tilde{\Delta}}{2(1+\tilde{u})}. \tag{B18}$$

The coefficients in Eq. (B17) are given by

$$c'_T = \frac{\pi^4}{12}\frac{1+2\tilde{u}^2+(1-\tilde{u})(5\tilde{u}-3)\tilde{\varepsilon}_d^2}{(1+\tilde{u})^2\left[1+(1-\tilde{u})^2\tilde{\varepsilon}_d^2\right]^2},$$

$$c'_B = \frac{\pi^2}{16}\frac{1-3(1-\tilde{u})^2\tilde{\varepsilon}_d^2}{\left[1+(1-\tilde{u})^2\tilde{\varepsilon}_d^2\right]^2},$$

where we have set $\tilde{\varepsilon}_d = \tilde{E}_d/\tilde{\Delta} = (\varepsilon_d + U/2)/\Delta$.

6. Derivation of the relation $\tilde{u} = R - 1$

From Fermi-liquid theory, we have the general result

$$\tilde{A}_{d,\sigma}(0) = z^{-1}A_{d,\sigma}(0) = \frac{\sin^2(\pi n_{d\sigma})}{\pi\tilde{\Delta}}, \tag{B19}$$

where z is the wave-function renormalization factor, and $n_{d\sigma}$ is the local level occupancy for spin σ. Along with this, we have the following Fermi-liquid relations for the specific heat, spin, and charge susceptibilities[28]:

$$\gamma_d = \frac{2\pi^2 k_B^2}{3}\tilde{A}_{d,\sigma}(0), \tag{B20}$$

$$\chi_d = \frac{(g\mu_B)^2}{2}\tilde{A}_{d,\sigma}(0)(1+\tilde{U}\tilde{A}_{d,\sigma}(0)), \tag{B21}$$

$$\chi_{c,d} = 2\tilde{A}_{d,\sigma}(0)(1-\tilde{U}\tilde{A}_{d,\sigma}(0)), \tag{B22}$$

where $\tilde{U} = z^2\Gamma_0$, $\tilde{\Delta} = z\Delta$. From Eqs. (B20)–(B22), we obtain

$$\frac{4}{(g\mu_B)^2}\chi_d + \chi_{c,d} = \frac{6}{\pi^2 k_B^2}\gamma_d, \tag{B23}$$

and together with the definition of the Wilson ratio, combined with Eqs. (B20)–(B23), we obtain

$$R \equiv \frac{4\pi^2 k_B^2}{3(g\mu_B)^2}\frac{\chi_d}{\gamma_d} = 1+\tilde{U}\tilde{A}_{d,\sigma}(0). \tag{B24}$$

Substituting Eq. (B19) into (B24), we obtain

$$R = 1 + \frac{\tilde{U}}{\pi\tilde{\Delta}}\sin^2(\pi n_{d\sigma}).$$

Let us define $\tilde{u} \equiv \tilde{U}/(\pi\tilde{\Delta}) = z\Gamma_0/(\pi\Delta)$, with Γ_0 defined by Eq. (B12) as the four-point vertex. Then, we have

$$\tilde{u} = \frac{R-1}{\sin^2(\pi n_{d\sigma})}. \tag{B25}$$

Finally, notice that for a particle-hole-symmetric system $n_{d\sigma} = \frac{1}{2}$, and hence $\tilde{u} = R - 1$.

[1] D. Goldhaber-Gordon, J. Göres, M. A. Kastner, H. Shtrikman, D. Mahalu, and U. Meirav, Phys. Rev. Lett. **81**, 5225 (1998).
[2] S. M. Cronenwett, T. H. Oosterkamp, and L. P. Kouwenhoven, Science **281**, 540 (1998).
[3] R. M. Potok, I. G. Rau, H. Shtrikman, Y. Oreg, and D. Goldhaber-Gordon, Nature (London) **446**, 167 (2007).
[4] A. V. Kretinin, H. Shtrikman, D. Goldhaber-Gordon, M. Hanl, A. Weichselbaum, J. von Delft, T. Costi, and D. Mahalu, Phys. Rev. B **84**, 245316 (2011).
[5] V. Madhavan, W. Chen, T. Jamneala, M. Crommie, and N. Wingreen, Science **280**, 567 (1998).
[6] A. Otte, M. Ternes, K. Von Bergmann, S. Loth, H. Brune, C. Lutz, C. Hirjibehedin, and A. Heinrich, Nat. Phys. **4**, 847 (2008).
[7] J. Li, W.-D. Schneider, R. Berndt, and B. Delley, Phys. Rev. Lett. **80**, 2893 (1998).
[8] J. Park, A. Pasupathy, J. Goldsmith, C. Chang, Y. Yaish, J. Petta, M. Rinkoski, J. Sethna, H. Abruna, P. McEuen, and D. Ralph, Nature (London) **417**, 722 (2002).
[9] L. H. Yu and D. Natelson, Nano Lett. **4**, 79 (2004).
[10] N. Roch, S. Florens, T. A. Costi, W. Wernsdorfer, and F. Balestro, Phys. Rev. Lett. **103**, 197202 (2009).
[11] J. J. Parks, A. R. Champagne, T. A. Costi, W. W. Shum, A. N. Pasupathy, E. Neuscamman, S. Flores-Torres, P. S. Cornaglia, A. A. Aligia, C. A. Balseiro, G. K.-L. Chan, H. D. Abruña, and D. C. Ralph, Science **328**, 1370 (2010).
[12] G. D. Scott, D. Natelson, S. Kirchner, and E. Muñoz, arXiv:1301.2168.
[13] A. C. Hewson, *The Kondo Problem to Heavy Fermions* (Cambridge University Press, Cambridge, 1997).
[14] S. Hershfield, Phys. Rev. Lett. **70**, 2134 (1993).
[15] M. H. Hettler, J. Kroha, and S. Hershfield, Phys. Rev. B **58**, 5649 (1998).
[16] A. Oguri, J. Phys. Soc. Jpn. **74**, 110 (2005).
[17] A. Rosch, J. Paaske, J. Kroha, and P. Wölfle, Phys. Rev. Lett. **90**, 076804 (2003).
[18] J. E. Han and R. J. Heary, Phys. Rev. Lett. **99**, 236808 (2007).
[19] P. Mehta and N. Andrei, Phys. Rev. Lett. **100**, 086804 (2008).
[20] F. B. Anders, Phys. Rev. Lett. **101**, 066804 (2008).
[21] Z. Ratiani and A. Mitra, Phys. Rev. B **79**, 245111 (2009).
[22] M. Pletyukhov and H. Schoeller, Phys. Rev. Lett. **108**, 260601 (2012).
[23] S. Smirnov and M. Grifoni, Phys. Rev. B **87**, 121302 (2013).
[24] A. A. Aligia, J. Phys.: Condens. Matter **24**, 015306 (2012).
[25] E. Muñoz, C. J. Bolech, and S. Kirchner, Phys. Rev. Lett. **110**, 016601 (2013).
[26] S. Kirchner, F. Zamani, and E. Muñoz, in *New Materials for Thermoelectric Applications: Theory and Experiment*, edited by V. Zlatić and A. C. Hewson, NATO Science for Peace and Security Series B: Physics and Biophysics, Vol. XX (Springer, Dordrecht, 2013), pp. 129–168.
[27] M. Grobis, I. G. Rau, R. M. Potok, H. Shtrikman, and D. Goldhaber-Gordon, Phys. Rev. Lett. **100**, 246601 (2008).
[28] A. C. Hewson, Phys. Rev. Lett. **70**, 4007 (1993).

[29] A. N. Rubtsov, M. I. Katsnelson, and A. I. Lichtenstein, Phys. Rev. B **77**, 033101 (2008).
[30] H. Hafermann, C. Jung, S. Brener, M. I. Katsnelson, A. N. Rubtsov, and A. I. Lichtenstein, Europhys. Lett. **85**, 27007 (2009).
[31] C. Jung, A. Lieder, S. Brener, H. Hafermann, B. Baxevanis, A. Chudnovskiy, A. Rubtsov, M. Katsnelson, and A. Lichtenstein, Ann. Phys. (Berlin) **524**, 49 (2012).
[32] K. G. Wilson, Rev. Mod. Phys. **47**, 773 (1975).
[33] H. R. Krishna-murthy, J. W. Wilkins, and K. G. Wilson, Phys. Rev. B **21**, 1003 (1980); **21**, 1044 (1980).
[34] R. Bulla, T. A. Costi, and T. Pruschke, Rev. Mod. Phys. **80**, 395 (2008).
[35] M. Yoshida, A. C. Seridonio, and L. N. Oliveira, Phys. Rev. B **80**, 235317 (2009).
[36] V. L. Campo and L. N. Oliveira, Phys. Rev. B **72**, 104432 (2005).
[37] R. Bulla, T. Pruschke, and A. C. Hewson, J. Phys.: Condens. Matter **9**, 10463 (1997).
[38] D. Goldhaber-Gordon, H. Shtrikman, D. Mahalu, D. Abusch-Magder, U. Meirav, and M. A. Kastner, Nature (London) **391**, 156 (1998).
[39] S. Hershfield, J. H. Davies, and J. W. Wilkins, Phys. Rev. Lett. **67**, 3720 (1991).
[40] Y. Meir, N. S. Wingreen, and P. A. Lee, Phys. Rev. Lett. **70**, 2601 (1993).
[41] O. Sakai, Y. Shimizu, and T. Kasuya, J. Phys. Soc. Jpn. **58**, 3666 (1989).
[42] R. Bulla, T. A. Costi, and D. Vollhardt, Phys. Rev. B **64**, 045103 (2001).
[43] A. Weichselbaum and J. von Delft, Phys. Rev. Lett. **99**, 076402 (2007)..
[44] R. Peters, T. Pruschke, and F. B. Anders, Phys. Rev. B **74**, 245114 (2006)
[45] F. B. Anders and A. Schiller, Phys. Rev. Lett. **95**, 196801 (2005).
[46] W. C. Oliveira and L. N. Oliveira, Phys. Rev. B **49**, 11986 (1994).
[47] The lower bound of this range $T_{\rm min} = 10^{-5} T_0$ is the lowest temperature for NRG calculations. Provided it is small enough, its precise value does not affect the quality of the fits significantly.
[48] A. C. Hewson, J. Bauer, and W. Koller, Phys. Rev. B **73**, 045117 (2006).
[49] P. Nozières, J. Low Temp. Phys. **17**, 31 (1974).
[50] T. A. Costi, A. C. Hewson, and V. Zlatić, J. Phys.: Condens. Matter **6**, 2519 (1994).
[51] R. M. Konik, H. Saleur, and A. Ludwig, Phys. Rev. B **66**, 125304 (2002).
[52] S. Hershfield, J. H. Davies, and J. W. Wilkins, Phys. Rev. B **46**, 7046 (1992).
[53] V. Zlatić and B. Horvatić, Phys. Rev. B **28**, 6904 (1983).
[54] A. M. Tsvelick and P. B. Wiegmann, J. Phys. C: Solid State Phys. **16**, 2321 (1983).
[55] A. Weichselbaum and M. Hanl find a similar value $T_{\rm K}^{\rm expt}/T_0^{(s)} \approx 1.06 \pm 0.03$ within a full density matrix approach to the spectral function (Ref. 43) (private communication). The present result improves on an earlier estimate for the $S = \frac{1}{2}$ Kondo model (Ref. 63) which yielded $T_{\rm K}^{\rm expt}/T_0^{(s)} \approx 0.94$.
[56] For example, $A_\Lambda = 1.41, 1.15, 1.04, 1.01$ for $\Lambda = 10, 4, 2, 1.5$.
[57] A different choice will be made later in Eq. (A7). At present, the only requirement on $\eta(\epsilon)$ is that $\eta(\pm D_\pm \Lambda^{-n-z}) = n$ and $\eta(\pm D_\pm \Lambda^{-n-1-z}) = n+1$, i.e., the boundaries of $[n, n+1]$ map onto the mesh points of the logarithmic grid.
[58] For $n = -1$ a similar expression applies on using $\epsilon = D_+ \Lambda^{-z(\eta+1)}$.
[59] Note that the derivation in Ref. 36 was actually for the two-impurity Anderson model, where the energy-dependent couplings arise via the nontrivial k dependence of the hybridization term $H_{\rm hyb} = V \sum_{\mathbf{k},j=1,2} (e^{i\mathbf{k}\hat{\mathbf{R}}_j} c_{\mathbf{k}}^\dagger d_j + \text{H.c.})$.
[60] O. Sakai and Y. Kuramoto, Solid State Commun. **89**, 307 (1994).
[61] R. Žitko and T. Pruschke, Phys. Rev. B **79**, 085106 (2009).
[62] A. Kamenev, arXiv:cond-mat/0412296 (unpublished).
[63] T. Micklitz, A. Altland, T. A. Costi, and A. Rosch, Phys. Rev. Lett. **96**, 226601 (2006).